DEPARTAMENTO DE CIÊNCIAS DA VIDA

FACULDADE DE CIÊNCIAS E TECNOLOGIA
UNIVERSIDADE DE COIMBRA

Characterization of new lanthanide complexes and nanoparticles as bimodal imaging agents

Dissertação apresentada à Universidade de Coimbra para cumprimento dos requisitos necessários à obtenção do grau de Mestre em Bioquímica, realizada sob a orientação científica do Professor Doutor Carlos F.G.C. Geraldes (Departamento de Ciências da Vida, Faculdade de Ciências e Tecnologia, Universidade de Coimbra)

Carlos Tadeu Barreirinhas Paula

2014

"Learn from yesterday, live for today, hope for tomorrow. The important thing is to not stop questioning."

Albert Einstein

Agradecimentos

Este momento marca o final de uma já longa etapa no meu percurso pessoal e académico. Longa não pelo tempo que encerra, mas por todas as vivências e aprendizagens que me proporcionou. 5 Anos, muitas pessoas, muitos ensinamentos. Urge, portanto, deixar alguns agradecimentos a todos aqueles que contribuíram para que este momento fosse possível.

Em primeiro lugar ao Professor Doutor Carlos F.G.C. Geraldes por me ter concedido a honra de trabalhar no seu grupo de investigação há já 3 anos. Por todo o apoio, espírito crítico, orientação científica e constante aconselhamento. Foi sem dúvida fundamental para o meu crescimento pessoal e académico e por tudo isso aqui deixo o meu mais sentido obrigado.

À Doutora Margarida Castro, porque sem saber, foi das pessoas mais essenciais para que este momento se concretizasse. Se não me tivesse colocado em contacto com o Professor Carlos Geraldes muito provavelmente nem estudante do Mestrado de Bioquímica seria. Agradeço pelo constante apoio que se seguiu a esse momento, e pela constante preocupação na construção de um curso de Bioquímica melhor.

Ao Doutor Emeric Wasielewski por todo o apoio técnico prestado na Unidade RMN.

Ao Doutor Fernando Hallwass e a Doutora Giovannia Pereira pela hospitalidade e por todo o acompanhamento científico concedido durante a minha estadia no Brasil.

Aos funcionários do Departamento de Ciências da Vida - Bioquímica, pela constante motivação que nos vão emprestando para conseguir atingir os nossos objectivos. São um exemplo de trabalho e parte importante do percurso de todos os estudantes.

Aos meus colegas e amigos, pelo constante apoio nas melhores e piores fases.

Finalmente, aos meus pais e família. Por todo tempo em que não pude estar presente, por todos os momentos em que não me deixaram desistir, por todo o apoio. São sem dúvida um modelo de referência e parte essencial de tudo o que conquistei.

Conto convosco para o que aí vem, porque a viagem só agora está a começar.

Resumo

A Imagem por Ressonância Magnética (IRM) é uma modalidade de imagem médica baseada em ressonância magnética nuclear (RMN), onde um mapa de sinais de ^{1}H NMR de uma determinada amostra é gerado. É uma excelente técnica de imagem, que permite a aquisição não-invasiva de imagens anatómicas de elevada resolução espacial. No entanto, a IRM tem como principal problema a sua baixa sensibilidade. Este inconveniente pode ser ultrapassado com a introdução de agentes externos que aumentem a intensidade de sinal. Estes agentes podem ser denominados agentes de contraste (AC) e pode ter várias formas. Uma dos tipos de moléculas mais vulgarmente utilizadas para induzir uma melhoria na intensidade do sinal são os complexos lantanídeos, sobretudo os complexos de Gd^{3+}.

Outra possível estratégia para melhorar a qualidade das imagens obtidas, consiste na combinação de diferentes métodos de imagem, a fim de criar um agente multimodal. Um dos campos de investigação mais usual é a bimodalidade Imagem óptica (IO)/IRM. A IO, devido às suas características, pode apresentar um ganho significativo em termos de sensibilidade. Os recentes avanços na nanotecnologia, mostrou que os *Quantum Dots* (QDs) são uma das aplicações mais promissoras da ciência dos materiais na Biologia. Eles podem ser utilizados na construção de AC para IO muito eficientes.

Neste trabalho é apresentada a construção de dois tipos de sistemas de imagem molecular. Em primeiro lugar, é relatado o estudo e caracterização de uma nova classe de AC para IRM baseados no bis(piridina-N-óxido) e sua possível aplicação a outros campos do RMN. Os resultados demonstram que a relaxividade dos complexos esta de acordo com resultados previamente descritos. Fica também provado que estes complexos apresentam um comportamento semelhante ao análogo que lhes deu origem, estando presentes essencialmente no isómero SAP. Os resultados indicam ainda que o ligando L2 produz os maiores desvios, sendo seguido pelo ligando L4. Ainda assim, mais detalhes terão que ser estudados para uma caracterização mais efectiva dos complexos.

Também se apresentam os estudos preliminares para a construção de um AC bimodal baseado em QDs e complexos de lantanídeos. Os resultados indicam que é possível criar estes agentes ainda que a estratégia de dopagem não seja a mais eficiente. Foi ainda provada e eficiência de conjugação com a Transferrina, indiciando assim a possibilidade de um agente de contraste com capacidade de vectorização.

PALAVRAS-CHAVE: AGENTES DE CONTRASTE PARA IRM, COMPLEXOS DE LANTANÍDEOS, AGENTES DE CONTRASTE BIMODAIS

Abstract

Magnetic Resonance Imaging (MRI) is an imaging modality based on Nuclear magnetic Resonance (NMR) where a map of ^{1}H NMR signals from a given sample is generated. It's an outstanding imaging technique, which allows the non-invasive acquisition of anatomical images with great spatial resolution. However, MRI is also a low sensitive technique. This drawback can be overcome with the introduction of external agents that increase the signal intensity. These agents can be named Contrast Agents (CAs) and can have various forms. One of the most commonly employed molecules to induce an improvement in signal intensity are the lanthanide complexes, mainly the Gd^{3+} complexes.

Another strategy to improve the image quality can be the combination of different imaging modalities, in order to create a multimodal agent. One of the most usual research frameworks are the bimodal Optical Imaging (OI)/MRI. OI, due to its characteristics, can introduce a great gain in sensitivity. Recent advances in nanotechnology, showed that Quantum Dots (QDs) are one of the most promising applications of material science to Biology. They can be used as highly efficient OI CAs.

In this work we focused on the construction of two types of systems for molecular imaging. Firstly, study and characterization of a MRI CAs based on bis(pyridine-N-oxide) and their possible application into other NMR fields.

The results show that the relaxivity of these complexes are in agreement with previously reported results. It is also proved that these complexes exhibit a similar chemical behavior than the analogue that gave rise to them, and are present mainly in the SAP isomer. The results further indicate that the ligand L2 produces the greatest shifts, followed by the ligand L4. Nonetheless more details will be studied for more effective characterization of the complexes.

It also presents the preliminary studies on the construction of a bimodal CA based on QD and lanthanide complexes. The results indicate that these agents can be created even if the doping strategy is not the most efficient. It was further tested the efficiency of bioconjugation with Transferrin, thereby indicating the possibility of a contrast agent capable of vectorization.

Keywords: MRI CONTRAST AGENTS; LANTHANIDE(III) COMPLEXES; BIMODAL IMAGING PROBES

INDEX

CHAPTER 1

General Introduction **1**

1.1-The Lanthanides **2**

1.2-Theory of Lanthanide-Induced NMR Shifts **5**

1.3-Molecular Imaging **9**

1.4-Magnetic Resonance imaging **11**

1.5-Basic Principles of MRI contrast agents **15**

1.6-Multimodal Imaging **25**

1.7-Nanoparticles for Molecular Imaging **27**

1.8-Optical Imaging **30**

1.9-Lanthanide Luminescence **32**

1.10-Quantum Dots in Biomedical Research **35**

CHAPTER 2

Materials and Methods **37**

2.1-Theory **38**

Longitudinal Relaxation Times 38

Bulk Magnetic Susceptibility 39

2.2-Experimental **40**

CHAPTER 3

Ln complexes analogues of DOTA: structural and relaxometric studies 43

3.1-Introduction 44

3.2-Results and Discussion 50

3.3-Conclusions 62

CHAPTER 4 67

QD doped with Gd^{3+}: a new class of Bimodal CAs 67

4.1-Introduction 68

4.2-Results and Discussion 69

4.3-Conclusions 72

References 75

CHAPTER I

General Introduction

1.1-The Lanthanides

The lanthanides are an exceptional group of fifteen elements ranging from lanthanum (Z=57) to lutetium (Z=71), with unique and distinctive physico-chemical and magnetic characteristics.[1]

Originally called as "rare earths" due to their natural occurrence as metal oxides, they are not particularly rare. The symbol Ln is used to refer any lanthanide. All but one of the lanthanides are f-block elements, with one to seven unpaired 4f electrons. Lutetium, a d-block element, is also considered to be a lanthanide due to its chemical similarities with the other fourteen. At physiological pH, they form stable trivalent ions (Ln^{3+}) in solution. As they are shielded by the 5s and 5p electrons, they are not readily available to form covalent interactions with ligands. Therefore, their interactions are largely electrostatic and the geometry of their complexes is usually determined by steric rather than by electronic factors. Another important consequence of this shielding is the large similarity in the chemical behavior of the 15 Ln^{3+} ions. Differences in chemical behavior may be ascribed to the decrease in ionic radius from La^{3+} to Lu^{3+}, a particular feature of these elements, the decrease in atomic size and radius with increasing atomic number, a property known as the lanthanide contraction.[2]

All lanthanide ions, with the exception La^{3+} and Lu^{3+} are paramagnetic. These two ions, with distinct magnetic properties, make a suitable reference of great importance in structural studies. Their paramagnetism gives raise to pronounced changes in chemical shifts of the nuclear spins located in their vicinities.

Another special character of this series is the Gadolinium ion (Gd^{3+}).[3] Gd^{3+} is the only paramagnetic lanthanide with isotropic environment due to the 7 unpaired electrons, and therefore, cannot produce an NMR dipolar shift in solution. Thus Gd^{3+} can only produce a contact shift. This particularity gives rise to a long electronic relaxation time that promotes strong relaxation enhancements in NMR spectra without changes in chemical shifts. The high efficiency of Gd^{3+} in nuclear relaxation led to successful introduction of Gd-based CA for MRI. Nowadays, the Gd-based contrast agents are the most used in the market, and still the ones more adequate for research development.

As far as it is known, the lanthanide ions do not have any essential role in biology. However due to its similar radius, Ln^{3+} can substitute Ca^{2+} in calcium binding proteins. This characteristic is really useful in structural biology once it permits the direct introduction of the probe in the protein without any structural change. It is also important to refer that due to the similar size of different Ln^{3+} ions, a binding site in a protein can bind different lanthanides with similar affinities, with only a minimum distortion in the protein.

Usually the various Ln^{3+} complexes of a particular ligand are nearly isostructural, although each of the ions has its own characteristic effect on the nucleus in its proximities.

The lanthanides produce varying paramagnetic effects, depending on the number of unpaired electrons. Some of them are strongly paramagnetic (Dy^{3+}, Tb^{3+}, Tm^{3+}) and others only moderate (Er^{3+}, Ho^{3+}, Yb^{3+}).

Lanthanide ions have been broadly used in a various types of applications in biological sciences. They have been used as luminescent chemosensors for biological imaging and analysis, catalysts for organic synthesis, anion sensors in aqueous solution, contrast agents for MRI, and as paramagnetic centers for high resolution nuclear magnetic resonance spectroscopy (NMR). These last two applications are the main outline of this thesis.

Among all the imaging techniques, Magnetic Resonance Imaging (MRI) is in many cases the imaging modality of choice. It has a high spatial resolution combined with low invasiveness and great tissue penetration. However, this technique has an inherently low sensitivity. On the other hand, optical and nuclear imaging provides a high sensitivity, but they have a low spatial resolution and in the case of optical imaging low tissue penetration. So, these techniques can be seen as complementary.

The lanthanide ions can combine these features, and be used in all these three imaging techniques, making them a unique class of CA that can yield multimodal signatures including, for example, long-lived fluorescence and magnetic resonance properties.

In NMR spectroscopy, paramagnetic lanthanides have been used as chemical shift mediators and line broadening agents to determine the conformation of biomolecules in solution since the 1970s.[4]

The use of these lanthanide ions to elucidate three-dimensional (3D) structures of proteins has been explored extensively.[5] These ions, due to their intrinsic paramagnetism offer outstanding opportunities for fast determination of 3D structures of protein-ligand complexes by NMR, which can be of great use in the development new and more specific drugs. They can be introduced in metalloproteins, eg. Ca^{2+} binding proteins, replacing Ca^{2+} by Ln^{3+} ion or extrinsically in non-metaloproteins by binding of a Ln^{3+}-ligand paramagnetic tag to amino-acid side chain of the protein . [6]

1.2-Theory of Lanthanide-Induced NMR Shifts

The Lanthanide-Induced NMR Shift (LIS) for a ligand nucleus uppon coordination with a Ln^{3+} ion (Δ) can be expressed as a sum of four components: the bulk magnetic susceptibility (BMS) shift (Δ_χ), the diamagnetic shift (Δ_d), the contact shift (Δ_c), and the pseudocontact (PCS) (Δ_p).[7] **Equation 1**

$$\Delta = \Delta_\chi + \Delta_d + \Delta_c + \Delta_p \qquad (1)$$

The BMS shift is usually not taken into account because it has no dependence on the structure of the compound, and thus has no relevant structural information. Each of the other three, mainly the contact and the pseudocontact shift, contain important information on the structure of Ln^{3+} complexes.

Diamagnetic shifts

This type of interactions is usually small and negligible. It originates from effects such as conformational changes, inductive effects and electrical field effects. In saturated ligands, these shifts are insignificant, with the exception of the nuclei directly coordinated to the Ln^{3+} ion.

Contact Shifts

This type of interaction arises from through-bond interactions of the unpaired electrons of the paramagnetic center and the nucleus under study. The magnitude of Δ_c decreases rapidly upon increase in the number of bonds between the Ln^{3+} ion and the nucleus, from the large values for the nucleus directly coordinated with the ion, allowing the determination of the donor sites in the ligand.

This value of Δ_c allows the determination of the stoichiometry of an LnL complex, and can be used in the development of new MRI contrast agents, once it enables the determination of the number of water molecules directly bonded to the Ln^{3+} ion center.

Pseudocontact Shifts

The pseudocontact shift (PCS) is a type of interaction induced by the paramagnetic lanthanide ions.[7] PCSs arise from the through-space dipolar interactions of the unpaired electrons of the paramagnetic center and it is the most useful type of lanthanide interaction in structural biochemistry.

It can be expressed by the **equation 2**:

$$\Delta p = \frac{1}{12\pi r^3}\left[\Delta\chi_{ax}(3cos^2\theta - 1) + \frac{3}{2}\Delta\chi_{rh}(sin^2\theta cos2\varphi)\right] \qquad (2)$$

where Δ_p is the difference in chemical shifts measured between diamagnetic and paramagnetic samples, r is the distance between the metal ion and the nuclear spin, $\Delta\chi_{ax}$ and $\Delta\chi_{rh}$ are the axial and rhombic components of the $\Delta\chi$ tensor, and the angles θ and ψ describe the position of the nuclear spin with respect to the principal axes of the magnetic susceptibility (χ) tensor.

The $\Delta\chi$ value is the anisotropy component of the magnetic susceptibility tensor χ of the metal ion. The χ tensor governs all paramagnetic effects, as it is shown on Figure 1.

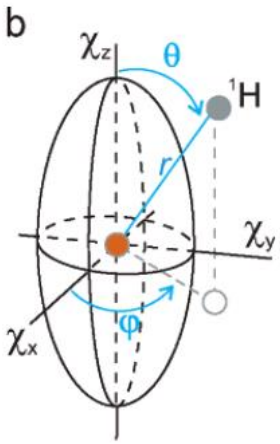

Figure 1.1- Schematic representation of the χ tensor. Adapted from [8]

The tensor χ can be decomposed into an isotropic component χ_{iso} and an anisotropic component, the $\Delta\chi$-tensor. The $\Delta\chi$-tensor is described by an axial ($\Delta\chi_{ax}$) and a rhombic ($\Delta\chi_{rh}$) component, according to **Equation 3**:

$$\Delta\chi_{ax} = \chi\chi_{zz} - \frac{\chi_{xx} + \chi_{yy}}{2} \; and \; \Delta\chi_{rh} = \chi_{xx} - \chi_{yy} \qquad (3)$$

These PCSs can be measured for nuclear spins as far as 40 Å from the metal ion.* It is more informative to visualize the PCSs as shells of constant PCS values, or "isosurfaces", plotted on the protein structure. A type of this schematic representation is shown on Figure 2.

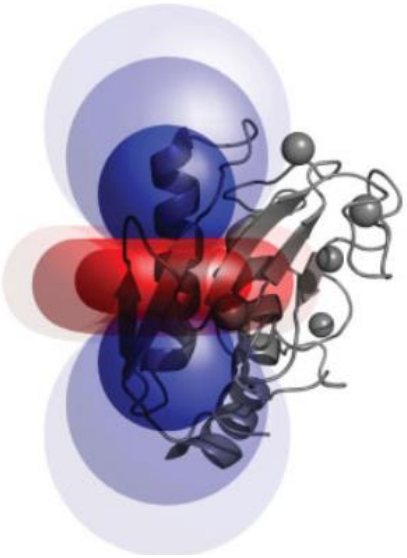

Figure 1.2- Isosurfaces representing the PCS induced by Yb^{3+} on catalytic domain of the MMP-1 protein. Adapted from [9]

Thus, these pseudocontact shifts due to the encoding of geometric and long-range distance information, provide a useful tool and unique opportunities in structural biology.

1.3-Molecular Imaging

Medical imaging can be defined as the set of processes and techniques used to image the human body for clinical proposes or for medical science. Molecular Imaging is a branch of Medical Imaging with particular focus on the molecular mechanisms of disease. This can also mean that through Molecular Imaging we try to do an in vivo characterization and measurement of biological processes at the cellular and molecular level, with great benefit for the patient by detecting disease at an early stage.[10]

Ever since Wilhelm Roentgen took the first X-ray of his wife's hand, in 1886, a new era has dawned for the field of medical imaging. A long road has been travelled since that date, and nowadays Molecular Imaging plays a vital role in the field of Medicine.

To date, six imaging techniques have emerged, allowing us to visualize targeted cells/molecules. Magnetic Resonance Imaging (MRI), Optical Imaging (OI), Ultrasound Imaging (US), X-ray Computed tomography (CT) and the nuclear imaging techniques: Positron Emission Tomography (PET) and Single Proton Emission Computed Tomography (SPECT). The main features of each technique are summarized at Table 1.

Table 1- Main features of the most relevant imaging techniques

Imaging technique	Disadvantages	Advantages	Possibility of human imaging
PET-SPECT	Low spatial resolution, radiation risks, high cost (for PET, cyclotron or generator needed)	High sensitivity, quantitative, no penetration limit	Yes
CT	Not quantitative, radiation risks, limited soft tissue resolution, limited molecular applications	Anatomical imaging, bone and tumor imaging	Yes
MRI	Low sensitivity, high cost, time consuming scan and processing	Morphological and functional imaging, no penetration limit, high spatial resolution	Yes
Optical Imaging	Photobleaching, limited penetration, low spatial	Low cost, easy manipulation, high	Yes, but limited

	resolution; autofluorescence disturbing	sensitivity, detection of fluorochrome in live and dead cells	
US	Limited resolution and sensitivity, low data reproducibility	Safety, low cost, wide availability, real time	Yes

As we can see from the table CT, US and MRI are intended to provide structural information, while more functional aspects are investigated by SPECT, PET and OI methods.

PET and SPECT are by far the most sensitive techniques, reaching the picomolar concentration. However, the exposure of the patients to ionizing radiation and its inherent low spatial resolution make the nuclear imaging techniques less favored than other imaging methods.

Among them MRI is the imaging modality of the moment. Unfortunately, the gain in resolution associated with MRI means a loss in sensitivity. The use of Contrast Agents (CAs) could help to overcome this drawback, by changing the relaxivity of water protons in their surroundings.

A lot of work has been done to improve the sensitivity of MRI, and in recent years the number of papers published on this subject is enormous.

One possible approach is the combination of various imaging techniques, constructing multimodal CAs that combine different imaging techniques in order to exploit the best of each imaging modality. Nowadays, scanners tend to house different imaging modalities, like for example PET/CT or PET/MRI. Together with the development of new multimodal CAs we are walking towards an improvement in diagnostic, and with that an improvement in healthcare.

Biomedical imaging research has leveraged the benefits of significant advances in electronics, information technology and, more recently, nanotechnology.

1.4-Magnetic Resonance imaging

Magnetic Resonance Imaging (MRI) is an imaging modality based on Nuclear magnetic Resonance (NMR) where a map of ^{1}H NMR signals from a given sample is generated. It's an outstanding imaging technique, which allows the non-invasive acquisition of anatomical images with great spatial resolution. The acquisition of images using the properties of NMR were first proposed by Raymond Damadian, in 1971, when he discovered that tumor tissues and healthy tissues had different water proton relaxation times.[11] By the same time, Paul Lauterbur had developed the first NMR imaging technique and obtained a "zeugmatogram", a cross-sectional image of two NMR tubes containing pure water and his work was later published in 1973. [12]

The relevance of MRI as consolidated imaging technique was later proved, in 2003, with the attribution of the Nobel Prize in Physiology or Medicine to Paul C. Lauterbour and Sir Peter Mansfield for "their discoveries concerning magnetic resonance imaging".

Today MRI is widely used in biomedical research due to its ability to obtain images with high spatial resolution and in hospitals worldwide as an essential diagnostic technique.

The images obtained from a MRI scanner arise from the water protons present in the tissues that represent more than 70% of the human body weight. Since the tissues and organs differ from each other in water content, images from the human body can be acquired.

The water ^{1}H nuclei are easily detected due to their high natural abundance in soft tissues and high relative sensibility of their NMR signal, given by**:**

$$\omega = \gamma_H B_0 \qquad (4)$$

where ω is their Larmor frequency, which is dependent on the proton giromagnetic ratio γ_H and on the applied homogenous magnetic field B_0.

The three dimensional spatial encoding is obtained through the application of linearly induced magnetic field gradients over the main homogenous magnetic field, thus for each proton nucleus in the sample we have:

$$\omega = \gamma_H(B_0 + G.r_i) \qquad (5)$$

where r_i represents the position of a given nucleus and G the vector representing the total gradient amplitude and direction (either G_x, G_y or G_z). This can be used for selectively obtain images from a slice portion of the sample. The two-dimensional image can then be obtained by either Back Projection Imaging or Fourier Transform Imaging, the latter being most commonly used.

To obtain clear and visible structures it is necessary to generate contrast between two image volume units (voxels). The Signal Intensity (SI) of each image voxel is dependent on four main factors: ^{1}H nuclei density or proton density (PD), spin lattice or longitudinal (T_1) and spin-spin or transversal (T_2) relaxation times and the water diffusion coefficient f(v). Proton density concerns the concentration of protons in given region. T_1 determines the rate of recovery of the longitudinal magnetization (M_z) to its equilibrium value (M_o) after a 90º pulse has made it zero, and the T_2 relaxation time determines the rate of disappearance of the transverse magnetization (M_{xy}) created by a pulse.

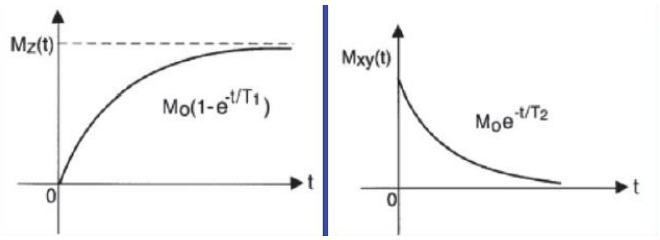

Figure 1- Longitudinal (T_1) and Transverse (T_2) relaxation curves.

The factors associated with the MRI scanner operation can also be changed in order to increase the image contrast. There are several pulse sequences, but Gradient Echo and Spin Echo are the most commonly employed in MRI measurements.

In order to determine T_1 it is usually used the pulse sequence inversion-recovery (Figure 1), and for T_2 determination the Carr-Purcell-Meiboom-Gill(CPGM), a spin echo pulse (Figure 2).

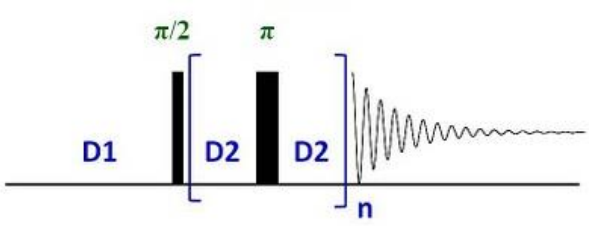

Figure 2- Carr-Purcell-Meiboom-Gill (CPGM) pulse sequence. Adapted from 5

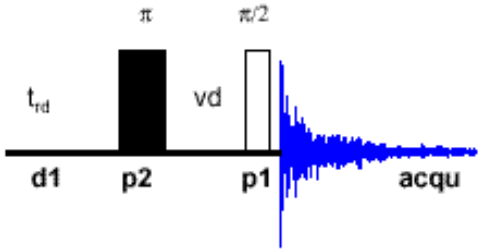

Figure 1.3- Inversion Recovery Pulse Sequence.

A simplified expression of the SI is given by **Equation 6**:

$$SI = \rho Hf(v)\left[1 - exp\left(\frac{-TR}{T1}\right)\right] exp\left(\frac{-TE}{T2}\right) \qquad (6)$$

where T_R is the time between two successive repetitions of the spin echo pulse sequence and T_E is the time between the first 90° pulse and the maximum of the acquired echo. As we can see from equation 6, by varying these two parameters the resulting image has different contributions of T1 or T2 and therefore it is possible to obtain three types of MR images. Either T_1-weighted (with shorter T_R values) or T_2-weighted (increased T_E values) Images.

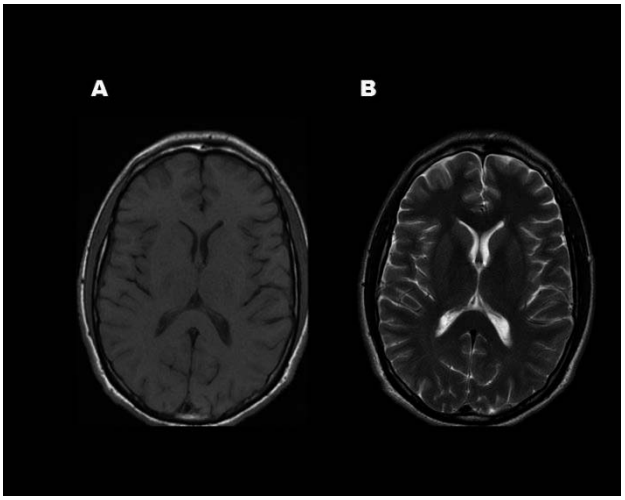

Figure 1.4- T_1 and T_2-weighted images. A- T_1-weighted; B- T_2-weighted.

Conventional T_1- and T_2-weighted Imaging modalities can be used to detect certain pathological processes, since either T_1 or T_2 times of a specific tissue can change as a result of certain biochemical events, such as variations in pH, temperature, salt or fat content.

External magnetic fields produced by the magnets in MRI scanners usually vary in the 1.5-11.7 T (Tesla) range, but the maximum magnetic field presently allowed for human use is 9.4T.

MR images can be produced without the introduction of any external agent to induce contrast between organs and tissues. However, some pathologies are better diagnosed when Contrast Agents (CA) are used, improving with it the possibility of a faster diagnose.

1.5-Basic Principles of MRI contrast agents

Contrast agents (CAs) for a variety of imaging methods have been used in Medicine for decades. MRI CAs are paramagnetic or superparamagnetic compounds that are able to modify the signal intensity by decreasing the T_1 and T_2 times of the water molecules in their vicinities.

These exogenous agents affect both T_1 and T_2 relaxation times. Though, the image contrast obtained depends on the dominant effect: decreased T_1 results on a positive contrast on T_1-weighted images while a decrease in T_2 results on a negative contrast on T_2-weighted images.

The signal enhancement produced by MRI CAs depends on their relaxivities (r_1 and r_2). The relaxivity can be defined as the increase of relaxation rates ($R_1=1/T_1$; $R_2=1/T_2$) produced by 1 mmol per liter of CA (expressed in s^{-1} mM) after the subtraction of the diamagnetic contribution. (**Equation 7**)

$$R_{i(Obs)} = \frac{1}{T_{i(obs)}} = \frac{1}{T_{i(diam)}} + r_i[CA]; \qquad i = 1 \; or \; 2 \qquad (7)$$

where $R_{i(obs)}$ is the global relaxation rate of the aqueous system (s^{-1}); $T_{i(diam)}$ relaxation time of the system before adding the CA; [CA] is the concentration of the contrast agent (mM) and r_i is the relaxivity (s^{-1} mM^{-1}).

There are two major contributions to paramagnetic relaxivity: “inner-sphere” and “outer-sphere” relaxation mechanisms as we can see from **Equation 8**.

$$r_i = r_i^{OS} + r_i^{IS}; \qquad i = 1 \; or \; 2 \qquad (8)$$

The principle of the “inner-sphere” relaxation process is represented in Figure 5, and is based on the relaxation effect originating from the closest hydrogen nuclei of

water molecules interacting directly with the paramagnetic center. The "inner-sphere" model has been described by the Solomon-Bloembergen-Morgan theory.[13]

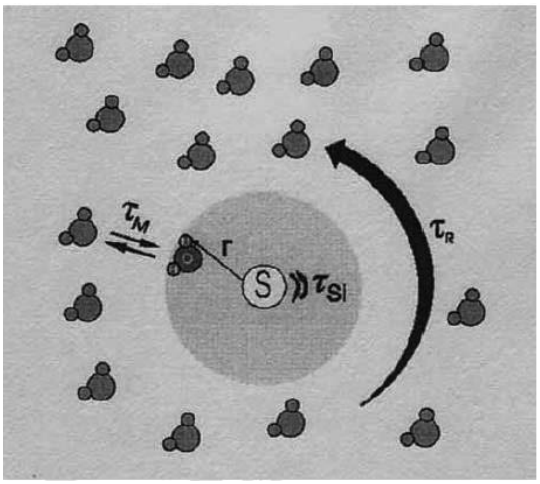

Figure 5- The inner-sphere relaxation mechanism. Adapted from [14]

The contribution of the "inner-sphere" mechanism to the relaxivity (R_i^{IS}) is given by **Equation 9**:

$$R_i^{IS} = fq\frac{1}{T_{1M}+\tau_M} \qquad (9)$$

Where f is the relative concentration of the paramagnetic center and of the water molecules; q is the number of water molecules in the first coordination sphere; T_{1M} is the longitudinal relaxation time of the bound water protons and τ_m is the water residence time.

The T_{1M} values are dominated by the molecular rotation time τ_r, the water residence time τ_m, and the number of coordinated water molecules (q). So, the slower the Gd^{3+} complex tumbles, the faster will be the relaxation rate. Thereby, these three parameters are the target of the researchers in order to produce more efficient CA.

The second contribution to paramagnetic relaxation is the "outer-sphere" relaxation. This type of interaction is due to the dipolar interaction at long-distance between the spin of the paramagnetic center and the nuclear spin. The "outer-sphere" model was described by Freed, and is modulated by the translational correlation time

(τ_d) that takes into account the relative diffusion (D) between the paramagnetic center and the solvent molecule, as well as their distance of closest approach d. Figure 6 shows a schematic representation of this type of interaction.

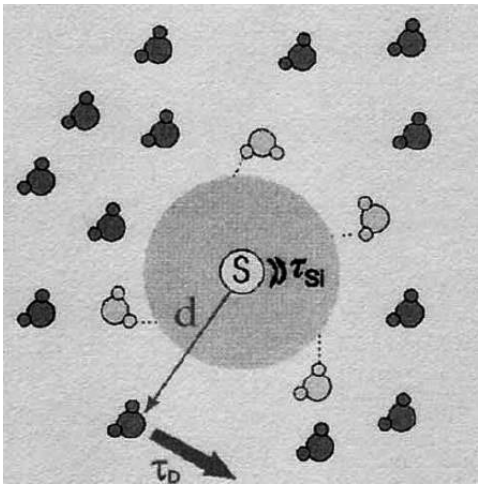

Figure 6- The outer-sphere relaxation mechanism. Adapted from [14]

For clinically approved CAs, approximately 60% of the relaxivity originates from inner sphere and 40% from outer sphere effects.

T_1 contrast agents (Positive agents)

Contrast agents that affect $_{T1}$ relaxation time are also called positive contrast agents, due to their ability to virtually increase the signal intensity in a $_{T1}$-weighted image. Lauterbur 's group stared this *in vivo* experiments using free Mn^{2+}, but soon it has become clear that this approach was highly toxic to living beings and so other paramagnetic metal ions since then, have been considered for MR imaging.[15] Other paramagnetic ions are still being continuously studied. Among them it is the gadolinium cation (Gd^{3+}). Due to is unique characteristics, Gd^{3+} soon started to get more interest for researchers. Gd^{3+} has a high magnetic moment (μ^2=63 BM^2), 7 unpaired f-electrons and long electronic relaxation times. Even though, the Gd^{3+} ion is extremely toxic even at very low doses. This toxicity is due to the previously reported capability to replace Ca^{2+} and block ionic channels and enzymatic processes. To avoid this toxicity, Gd^{3+} must be coordinated to specific ligands, able to form thermodynamically very stable and

kinetically inert complexes. The stability of the Gd^{3+} complexes is a very important requirement to avoid the release if free metal ion into the body.

The majority of the clinically approved T_1 contrast agents are gadolinium-based and formed with polyaminoarboxylate ligands, such as DOTA. The Clinically approved T_1-Contrast agents are summarized at Table 2.

Table 2- Clinically approved T_1-Contrast agents.[16]

Commercial Name	Chemical Name	Generic Name	Manufacturer	$r_1(mM^{-1}s^{-1})$
Gadovist	Gd-BT-DO3A	Gadobutrol	Bayer	5.2
Gadodiamide	Gd-DTPA-BMA	Gadidiamide	GE Healthcare	4.3
Gadopentate dimeglumine	Magnevist	Gd-DTPA	Bayer	4.1
Gadoterate meglumine	Dotarem	Gd-DOTA	Guerbet	3.6
Gadoteridol	ProHance	Gd-HDO3A	Bracco	4.1
Gadoversetamine	Optimark	Gd-DTPA-BMEA	Mallinckrodt	4.7
Gadobenate dimeglumine	Multihence	Gd-BOPTA	Bracco	6.3
Gadoxetate disodium	Eovist	Gd-EOB-DTPA	Bayer	6.9

As mentioned above, the efficiency of a CA is expressed by its relaxivity. Commercially available Gd^{3+} contrast agents have relaxivities of 4-5 $s^{-1}mM^{-1}$ at a typical clinical magnetic field strengths (1.5T), consequently inducing a poor enhancement in a MR image. This is where the organic chemists intervene, to develop newer strategies that could improve not only the relaxivity, but also the target capability of a contrast agent.

The perfect CA should be highly stable and have the capacity to enhance the relaxation rate of the solvent protons to their potential maximum.

There are several molecular parameters that we can improve to create a more efficient CA. These include the number of water molecules directly coordinated with the metal ion (q); the exchange lifetime of those molecules (τ_M) and the re-orientational correlation time (τ_R) of the complex.[15]

The number of water molecules (q) is typically one due to the high stability of the complexes produced with this design. These types of Gd^{3+} complexes usually adopt an octahedral geometry, which hosts nine donor atoms in its coordination sphere allowing the creation of a very stable complex and preventing the realising of the Gd^{3+} ion.

Several groups have been working extensively on the development of new complexes with a q value greater than one. But so far, mainly by thermodynamic and stability factors, none of them have been approved for clinical use.

The molecular rotational correlation time, τ_R, mainly depends on the molecular radius of the complex, and thus higher molecular weight induces a lengthening of the τ_R which consequently leads to a higher relaxivity.

A lot of work has been developed to increase the τ_R parameter, for instance, by covalently or non-covalently binding the complexes to macromolecules.

The clinically approved Vasovist was the first example of a CA with a boost on this particular parameter. Vasovist strongly and non-covalently binds to the serum albumin protein, which results in a significant increase in the relaxivity and in the lifetime in the vasculature stream.

Lastly, the exchange lifetime of the water molecules, τ_M, is also a crucial parameter that affects the observed relaxivity. An excessively slow τ_M has a disadvantageous effect on r_1, essentially because the effect of the paramagnetism is inefficiently passed to the bulk water, whereas a fast water exchange has the same effect on r_1, as the water molecules are not in contact long enough with the paramagnetic ion, so do not experience its effect.

This parameter is strongly affected by several factors that influence the water exchange mechanism. These include the nature of the coordination arms, the overall charge of the complex and the presence of bulky substituents which destabilize the complex structure relative to its transition state and thus promote a water dissociative mechanism.[13] This value can be obtained from the fitting the temperature dependence profiles of the transverse relaxation rate of ^{17}O labelled water.[13]

Another class of T_1 contrast agents that are increasing their relevance in the MRI field are the responsive agents. A responsive agent is capable of reporting a metabolic or physiological event by altering its relaxivity with it. Examples of responsive MRI contrast agents include: enzymatically activated CAs; CAs sensitive to pH, temperature, radicals, oxygen partial pressure, or metal ion concentration.[16]

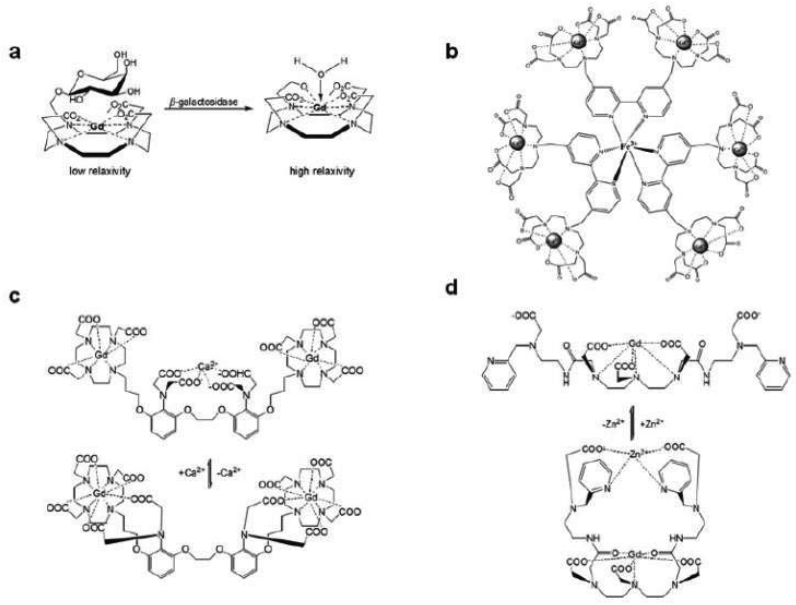

Figure 7- Examples of some Gd^{3+} complexes reported as responsive MRI CAs.

Responsive agents are on the line to be astonishing and crucial tools in molecular diagnostics, though several issues, such as the difficult direct correlation between a relaxivity change and a physiological even must be overcome to confirm their great potential.

T_2 Contrast agents

T_2 contrast agents decrease the water signal intensity by shortening the transverse relaxation times. The large magnetic susceptibility anisotropies induced by these agents are able to create local magnetic fields gradients in solution, which efficiently diphase the transverse magnetization components.

The advent of MRI scanners with more powerful magnets offers a challenge to the scientific community, once T_1contrast agents become less efficient at high magnetic fields due to the decrease of r_1 relaxivity with increasing field.

On the other hand, T_2 contrast agents can be efficient at high fields since the transverse relaxivity (r_2) increases at high fields, as can be seen by the relaxation time (T_2) dependence on the square of Bo (**Equation 10**). So, the improvement in the techniques of production of MRI scanners is pulling through the development of better T_2 contrast agents.

$$\frac{1}{T_2} = fq\frac{\tau_m\ \Delta\omega_M^2}{1+\tau_m^2\,\Delta\omega_M^2} \qquad (10)$$

At the present time, the majority of T_2 contrast agents are iron-oxide based, named as superparamagnetic iron oxide nanoparticles (SPIO). SPIOs usually consist of a magnetite (Fe_3O_4) or maghemite (γFe_2O_3) core, coated with a natural or synthetic polymer and can be characterized according to their mean size. They can be divided into three main categories: Oral SPIO, Stantard SPIO (SSPIO) and Ultrasmall SPIO (USPIO). The commercially available Iron-oxide based CAs are resumed in Table 3.

Table 3- Commercially available Iron-oxide base Nanoparticles.

Classification	Trade Name	Coating Material	Hydrodynamic Diameter
Oral SPIO	Lumirem	Silicon	300 nm
	Abdoscan	Sulphonated Styrene	3.5 μm
	Endorem	Dextran	80-180 nm
SSPIO	Resovist	Carboxydrextran	60 nm
	Clariscan	Pegylated Starch	20 nm
USPIO	Supravist	Carboxydextran	30 nm
	Sinerem	Dextran	15-40 nm

The low toxicity of SPIOs allows their application in imaging procedures, such as macrophage infiltration in inflammatory regions, cancer diagnosis and the early detection of cardiovascular diseases. Nevertheless, the most promising application of this type of contrast agents concerns the detection of the fate of cells in vivo, after their previous labelling.[16]

Paramagnetic liposomes can also be included in the class of T_2 agents and their effect mainly depends on the magnetic moment of the paramagnetic complexes, on the amount of agent entrapped in the vesicle as well as on its dimensions and the magnetic field. Still, few reports are available in the literature on such systems.

Recently, many novel systems have been studied as potential T_2 contrast agents such as carbon nanotubes, zeolites and metal-organic frameworks.[16]

Other classifications

The continuous search for the ideal CAs, led to a wide amount of data that need to be properly classified, in order to be useful for the scientific community.

MRI contrast agents can be listed in several ways, such as (1) the presence and the nature of their metal center, (2) their magnetic properties, (3) their effect on image, (4) their chemical structure and ligands present and finally (5) their biodistribution and applications.[16]

According to their biodistribution and applications the CAs can also be divided into five main classes or groups: (a) Non-specific extracellular agents, (b) Blood pool agents, (c) Organ-specific agents (d) Targeting agents and (e) Responsive agents. They are all summarized in Table 4.

Table 4- Classification of Contrast Agents according to their Biodistribution.

Classification	Characteristics	Examples
Non-specific extracellular agents	After intravenous injection, leak from the blood pool into the interstitial space due to their small molecular weight. These agents do not have the ability to cross an intact blood-brain barrier. They provide visualization of regions with abnormally high permeability, such as tumors or lesions.	Magnevist®, Dotarem®, Omniscan®, ProHance®, Gadovist®, MultiHance® and OptiMARK®.
Blood Pool Agents	Agents in this class have higher molecular weight than those in the previous class, a fact that prevents their release into the interstitial space and so they remain for longer	Vasovist®, Vistarem®, Sinerem®, Combidex® and

	periods in the blood stream. This characteristic allows the imaging of the vasculature.	Supravist®.
Organ-Specific agents	Existing contrast agents that have a natural tendency to be internalized by a specific cell type.	Primovist®, Eovist®, Tealascan®, Feridex®, Endorem®, Resovist®,
Targeting agents	These agents are able to recognize specific moieties on the cell surface. Although this is a rather elegant methodology, it suffers from low target area concentration, making it difficult to achieve sufficient contrast. Nevertheless, targeted nanoparticles seem to be a way of overcoming this major drawback.	Liposomes with RGD moiety associated, for neovasculature targeting; Liposomes functionalized with folate
Responsive agents	These so-called “smart agents” are sensitive to certain stimuli that include pH, enzymatic activity, redox potential, etc, allowing the characterization of the microenvironment of the region of the interest to be achieved.	Egad, Gd-DOTAserotonin

1.6-Multimodal Imaging

As seen earlier, MRI is defined as a low sensitive technique which requires in most cases the use of Contrast Agents to enhance the signal. But sometimes even that isn't enough to get good results making the validation of *in vivo* imaging experiments by more than one approach essential. Therefore the development of CAs that combine more than one imaging technique is essential to perform better results.

Building on this idea the concept of multimodal imaging arose. Multimodal imaging can be defined as the merger on a single CAs of several features of diverse imaging techniques to provide complementary information in biological studies and medical diagnostics.[17] Multimodal CAs enable the colocalization of the acquired images by at least two modalities and provide a powerful way to validate *in vivo* molecular imaging experiments.

Radioactive tracers and optical imaging CAs are orders of magnitude more sensitive than MRI CAs and can be detected at extremely low concentrations (picomolar in the case of PET, when MRI CAs can only detect at milimolar concentrations). Thus, to improve the results of an usual MRI scan, the development of multimodal probes that combine one or imaging techniques is essential.

One of the most employed multimodal approaches is the combination of MRI and Optical Imaging. Optical imaging CAs are far more sensitive than MRI CAs and the complementarity of the techniques can provide better results. Hence, the development of bimodal OI/MRI contrast agents is pressing.

Bimodal CAs OI/MRI combine the high spatial and temporal resolution and deep tissue penetration of MRI, with the high sensitivity of OI.

Several strategies have been tried so far to obtain efficient bimodal MRI/OI contrast agents. These strategies can be roughly divided into three classes: T1 contrast agents covalently bound to a fluorescent molecule; T1 agents and flurophore associated nonconvalently; T2 agents covalently bound to a fluorescent probe.[17]

The first example of an MRI/Optical imaging probe appeared in 1998. Hueber and is colleagues prepared one monomeric and two polymeric multimodal probes based on MRI CAs conjugated to tetramelhylrhodamine. [18]

Mulder on its article in 2006, revealed that Quantum Dots (QDs) can be functionalized with paramagnetic ions to produce in this way a multimodal probe that can be detected by both MRI and fluorescence microscopy.[19]

These are just some of the examples that the Multimodal Imaging could play a key role on the field of Molecular Imaging.

1.7-Nanoparticles for Molecular Imaging

Nanotechnology may be defined as the understanding and control of the matter between 1-100 nm size range. The application of nanotechnology to the field of medicine can be called as nanomedicine and concerns on the engineering of these materials to improve diagnostic and therapeutic techniques.[20,21]

Nanotechnology has experienced a high development over the last decade. This field of science opens new insights in broad range of domains, and MRI is not an exception. The idea of using nanoparticles as MRI contrast agents appeared in the 70s, but with recent advances in the field nanotechnology a new interest has woken up the researchers worldwide.

Nanoparticles can be used to enhance sensitivity of MRI images, but also to enable modulation of energy in the form of light, sound or electron beams in some type of treatments (e.g. hypertermal therapy), as well as drugs carriers. [20]

One of the most successful applications of nanotechnology are the Magnetic Nanoparticles (MN). The most commonly used nanoparticles in MRI are the superparamagnetic iron-oxide nanoparticles (SPIONs), that have been used for two decades. It was the first nanoparticulate MRI contrast agent, and is still used these days in clinic.

These nanoparticles-based MRI contrast agents are composed of three main parts: (1) the core nanoparticle, which is responsible for the contrast enhancement; (2) the water-dispersible shells, which provide a better biodistribution; and finally (3) the bioactive materials for targeting propose. The structure of an MRI contrast agent is shown on Figure 8.

Nowadays, MRI contrast agents typically in use range from 5 nm to several microns in diameter.

Physically, they can be classified into two major categories: (1) Liquid and (2) Solid. Liquid particles include Liposomes, Micelles and perfluorocarbon emulsions. These liquid nanoparticles can be passively targeted, or functionalized by complexing lipophilic targeting agents to their outer lipid membrane or in their cores. They can get

their paramagnetic properties by incorporating lipophilic gadolinium chelates in the membrane. Depending on the size of the particle, a great amplification can be achieved, because many Gd^{3+} ions can be carried in a single particle.

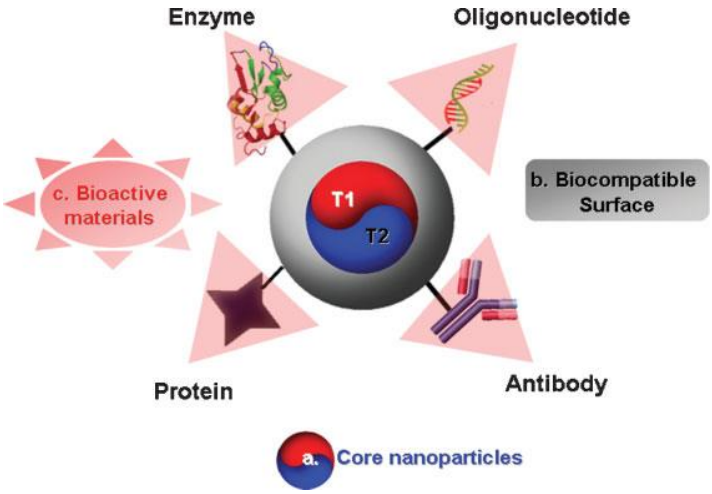

Figure 8- General scheme of a Nanoparticle used in molecular imaging. [22]

Solid nanoparticles include the family of iron oxide particles. In this group are included the micrometer-sized paramagnetic iron oxide particles (MPIO), superparamagnetic iron oxide particles (SPIO; 50-500 nm) and ultrasmall superparamagnetic iron oxide particles (USPIO; 5-50 nm). These particles are generally coated with polymers, to maintain their solubility and reduce particle agglomeration. These SPIO particles consist of multiple iron oxide cores within a dextran stabilization shell.

Cross-linked iron oxide particles (CLIO) have functionalised surfaces which can accept targeting ligands, so they can be specifically targeted.

The usual targets of SPIOs have been liver diseases, because SPIOs are selectively taken up by the Kupffer cells in the liver, spleen and bone marrow. If a normal liver is damaged by a tumor or any other disease, the levels of Kupffer cell are decreased in the injured region. Due to the negligible uptake by the abnormal liver,

SPIOs show a great contrast between normal and injured tissue, thereby permitting a clear detection of the abnormal tissue. However, SPIOs uptake by the liver leads to rapid excretion from the blood plasma, which induces a limitation to the SPIOs ability for detection of molecular and biological features.

The efficacy and stability of the nanoparticles depends on several parameters such as the size of the iron oxide crystal, their hydrodynamic size, charge and coating.

The size of particles is the main factor that controls their characteristics, such as biodistribution and blood half-life. Small nanoparticles have a longer plasma circulation, due to its slow excretion from the liver. Therefore, USPIO are the most favourable for molecular imaging studies. A typical clinical application for USPIO is lymph-node imaging. Among other applications USPIOs have been tested as blood-pool agents because they are readily distributed in the extracellular intravascular space. For example, USPIOs have been tested for application in angiography, functional MRI and passive targeted tumor imaging.

Nanosized particles can easily uptaken by both macrophages and nonphagocytic cells. Furthermore, due to their characteristics nanoparticles can be targeted because of their large surface area that can be conjugated with biological and targeting agents, such as antibodies, oligonucleotides, aptamers, or others, which opens great opportunities for their application.

Therefore, iron oxide particles have already shown outstanding results in the field of targeted-specific *in vivo* and *in vitro* molecular imaging, in particular in monitoring the migration and tracking cells and in diseased targeted-imaging.

1.8-Optical Imaging

Light in the IR-Vis-UV range is the most versatile form of radiation. It is non-invasive and able to create a contrast by intensity, wavelength, polarization, coherence, interference lifetime and nonlinear effects. Optical imaging (OI) techniques have different physical parameters of light interaction.

Optical imaging can be divided into two main techniques: *in vivo* fluorescence imaging and bioluminescence imaging (BLI).

Among the optical imaging techniques available, fluorescence microscopy has emerged as one of the most powerful imaging techniques.[23] Optical fluorescence depends on the inherent properties if the fluorophore, which can be, as an example, organic dyes or lanthanide compounds.

When a fluorophore is excited by quanta of specific energy, it excites electrons from the ground state to a higher energy singlet state (S_1, S_2). Since different electrons have different energies (rotational and vibrational), the transition to a singlet state demands change to an equivalent vibrational or rotational energy at a higher electrical state. During this process, the electron loses a part of its energy, generally through thermal decay (non-radiative energy decay) and, as a result, a lower energy photon is emitted. The difference between the wavelength required for excitation and the wavelength of the emitted light is known as the Stokes shift. This is the essential basis of all fluorescence methods. This process is summarized at **Figure 9**

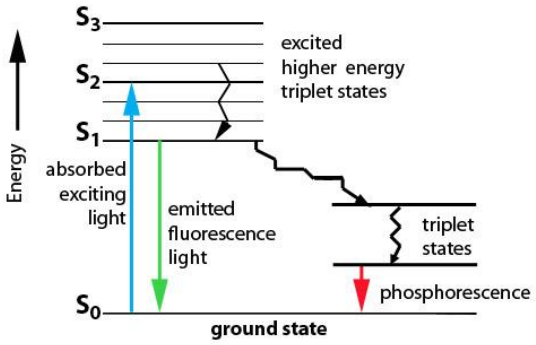

Figure 1.9- Schematic representation of the fluorescence process.

Another very relevant optical imaging technique is Near-Infrared (NIR) fluorescence imaging. NIR fluorescence imaging is usually used for *in vivo* applications because hemoglobin, water, and lipids have the lowest absorption coefficient in the NIR region (650-900 nm) allowing deep tissue penetration. Moreover, NIR signal detection takes advantage of minimal tissue autofluorescence thus increasing the signal-to-noise ratio. As NIR light diffracts much less than visible light, NIR optical is also a way to improve high resolution pictures of deep tissues.

Optical imaging is a low cost technique, possesses nanomolar sensitivity, as a great variety of probes already established and allows multichannel imaging using multiple probes with different spectral properties. Even so, Optical imaging like any other imaging technique has some limitations. Poor spatial resolution, autofluorescence and low ability to obtain quantitative information in vivo caused by limitation in penetration and scattering if light in the tissue can by appointed as examples of some of these drawbacks.

Once again, a possible solution to overcome these limitations may be the resource to multimodal imaging.

1.9-Lanthanide Luminescence

Trivalent lanthanide ions also present a good alternative to organic dyes due to their singular properties and the ability to be easily detected at a visible and NIR range.[24]

The first staining of biological cells with lanthanides dates back to 1969 when bacterial smears (Escherichia coli cell walls) were treated with aqueous ethanolic solutions of europium[25], but further experiments had to wait a long time.

Luminescent properties of lanthanide ions derive from their characteristic $[Xe]4f^n$ (n = 0-14) electronic configuration, which is responsible for a great number of electronic levels [14!/n!(14-n)!]. They can be characterized by three quantum numbers (S, L and J) with well-defined energy levels due to shielding of the 4f orbitals by the filled $5s^2 5p^6$ subshells, and are a little sensitive to the chemical environments where the lanthanides are inserted. The resulting parity forbidden 4f-4f transitions are sharp and characteristic of each Ln^{III} ion, allowing for better discrimination from background fluorescence and realization of time-resolved experiments due to long life-times of the excited states.

Therefore, the emissive properties of these compounds can be modified by simple Ln^{III} ion substitution, straddling from Gd^{III} (UV) to Eu^{III} and Tb^{III} (UV-Vis) and to Nd^{III} and Yb^{III} (Near-Infrared Region - NIR), thus allowing for multiplex assays. (**Figure 10)**

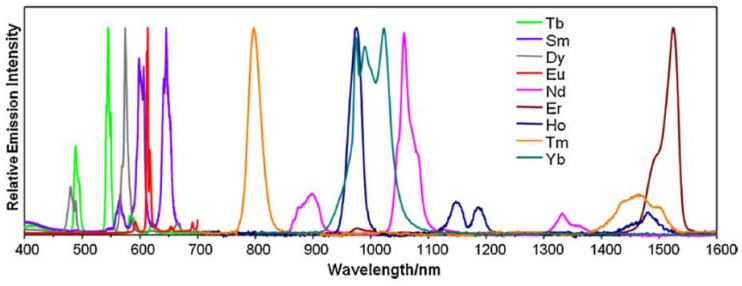

Figure 1.10- Normalized emission spectra of luminescent lanthanide complexes in solution.[26]

An additional advantage of lanthanide complexes in relation to organic dyes is their good resistance to photobleaching. However, the very low Intrinsic Quantum Yields of Ln^{III} can be seen has a drawback.

The Intrinsic Quantum Yield corresponds to the ratio between the number of emitted photons and the number of absorbed photons by a Ln^{III} ion and can be calculated by taking into account the life-time of the excited state τ_{obs}, the corresponding rate of de-population of the excited state k_{obs} (s^{-1}) (τ_{obs}= 1/ k_{obs}) and the radiative rate constant k^{rad}:

$$Q_{Ln}^{Ln} = \frac{k^{rad}}{k_{obs}} \qquad (11)$$

A possible way to overcome the weak emission of the Ln^{III}, involves the combination of the metal with organic molecules, where excitation in the ligand region leads to a metal-centered luminescence. This effect known as "Antenna Effect" or Sensitization Luminescence, happens when part of the energy absorbed by the organic ligand is transferred to the Ln^{III} exited states, giving origin to sharp bands that correspond to internal conversion to the emitting level.

Therefore, a new concept emerges from it: the overall Quantum Yields (Q_{Ln}^{L}), which corresponds to the obtained Quantum Yields in the presence of an energy donor, such as the organic ligands mentioned above, and can be describe by Equation 12:

$$Q_{Ln}^{L} = \eta_{sens} Q_{Ln}^{Ln} \qquad (12)$$

where η_{sens} represents the sensitization efficiency, which can be described by:

$$\eta_{sens} = \eta_{pop}^{D} \eta_{et} \qquad (13)$$

where η_{pop}^{D} is the efficiency with which the feeding level is populated and η_{et} the efficiency of energy transfer from donor to the accepting level.

The design of new lanthanide complexes with high emissive rates needs to take into account these two parameters.

1.10-Quantum Dots in Biomedical Research

One of the most rapidly evolving fields in nanotechnology is the use of Quantum Dots in Biology.

Quantum Dots (QDs) are colloidal semiconductor nanocrystals with unique optical properties due to their three dimensional quantum confinement regime. Their diameter usually ranges from 2 to 10 nm, and consists in a semiconductor particle named "core", that is usually coated by a layer of another semiconductor material named "shell". **Figure 11**

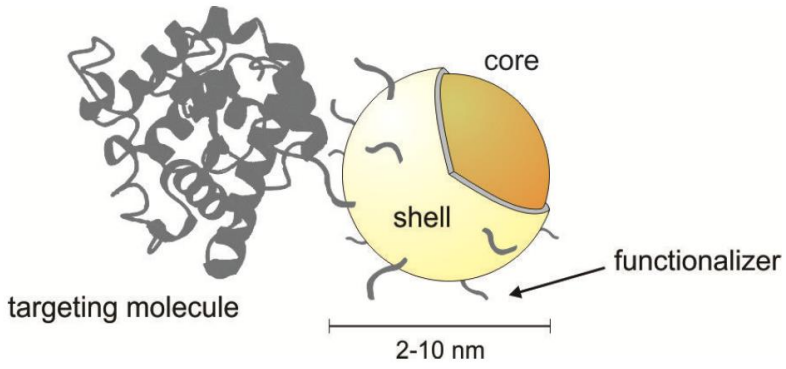

Figure 1.11- General scheme of a Quantum dot linked to a biomolecule.[27]

The QD core is responsible for the fundamental optical properties, and the shell is mainly used to passivate the surface of the core, improving its optical properties and preventing chemical attack. Thus, the shell separates physically the core, optically active, from the medium. As consequence, the optical properties of the QD are less sensitive to changes, like pH or oxygen presence.

For biomedical purposes, fluorescence in the visible region is usually required, both core and shell are composed of elements from the II B and VI A groups of the periodic table. The major examples are CdSe/ZnS, CdTe/CdS and ZnSe/ZnS QDs.

QDs were firstly used for cell imaging in 1998 by Nie's and Alivisatos's group[28], and since then their applications have been extended. QDs provide a new class of biomarkers that can overcome the limitations of organic dyes.[23] Compared to conventional fluorophores, QDs are photochemically stable, brighter, have a narrow, tunable and symmetric emission spectrum, and are metabolically stable. There are, however, some issues associated with these materials. The problem of acute toxicity and photo-oxidation can be overcome as referred earlier by capping the particle with a protective shell of insulating material or semiconductor, for example, ZnS-coated CdSe Core/shell QDs.[29] Water solubility is also a key parameter for their applications as imaging agents. A wide range of methods has been reported to achieve this, such as fabricating the surface with suitable thiolated ligands, over-coating with silica, and encapsulating with amine-modified polymers.

An important feature of these nanosystems is their ability to be functionalized, thereby allowing the incorporation of new properties such as vectorization or another imaging modality.

QDs can be doped with paramagnetic ions such as Gd^{3+} or Mn^{2+} giving them the ability to be detected by MRI. This can be also done by functionalizing the surface of QDs with organic chelates containing paramagnetic ions. Despite further works of this type have been already reported, in this project we will use a well-established type of organic chelates,[30,31] allowing the development of an interesting bimodal probe based on nanotechnology.

CHAPTER 2

Materials and Methods

2.1-Theory

Longitudinal Relaxation Times

The relaxation of ^1H nuclei can be described under the basic principles of NMR spectroscopy. For a sample containing ^1H nuclei placed in an effective magnetic field B_0 oriented along the zz axis, a magnetic component M_z is created, corresponding to the overall contribution of all sample spins. An M_{xy} component is created with the application of a perpendicular RF pulse (B_1) in relation to B_0 that evolves again to the zz axis. This return to the thermal equilibrium, defined by the Boltzmann equation, is called nuclear spin relaxation. As described in chapter one, this can occur through two different mechanisms that are characteristic for each non-equivalent spins in the sample, namely the longitudinal (T_1) and transversal (T_2) relaxation.

In relaxometric studies we take into account the water protons of a given sample.

Determination of longitudinal relaxation times is done with the inversion-recovery pulse sequence. (Figure 2.1)

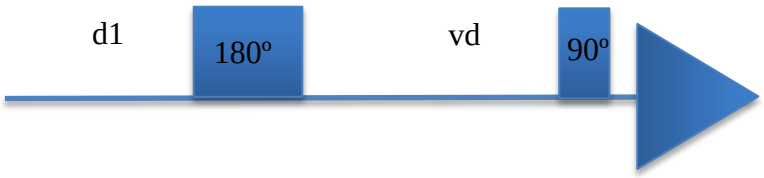

Figure 2.1-Schematic representation of the Inversion-recovery pulse sequence.

where 180° represents a 180° RF pulse, after a delay period d1, that leads to an inversion of spin populations, vd represents the variable delay time that corresponds to M_z evolution and 90° represents a 90° RF pulse that allows the acquisition of a M_{xy}

component corresponding to M_z. The T_1 values and evolution of the magnetization vectors are described by the Bloch equations.[32]

Bulk Magnetic Susceptibility

The Bulk Magnetic Susceptibility (BMS) method, or Evans method, is a simple method to measure the concentration of a paramagnetic species in solution.[33] It is based on the bulk magnetic susceptibility shift ($\Delta\chi$) which is expressed by **Equation 14**.

$$\Delta\chi = \frac{4\pi cs}{T}\left(\frac{\mu_{eff}}{2.84}\right)^2 \times 10^3 \qquad (14)$$

where c is the concentration of the paramagnetic species (mol^{-1}), s is a parameter dependent on the shape of the sample and its relative position relative to the magnetic field (s = 1/3 for cilindric samples), T is the absolute temperature and μ_{eff} is the effective magnetic moment of the lanthanide ion, which for Gd^{3+} : μ_{eff} 7.94 μB.[34]

In this technique a sample containing the paramagnetic compound and 10% t-butanol solution is placed in a NMR tube and the frequency shift of t-butanol is determined by comparison with a diamagnetic solution containing the same solvent and percentage of t-butanol.

2.2-Experimental

Materials and reagents

Ln^{3+} salts were obtained from Sigma-Aldrich and used with no further purification. Solvents (MilliQ water and D_2O) were used with no further purification. The ligands were synthesized and purified in the Leiden Institute of Chemistry, Leiden University and gently supplied by Dr. Wei Min Liu and Prof. Marcellus Ubbink. L1 and L3 samples Lu, Yb, Tm, Tb, Gd and Eu were received in 2 mM and 10mM D_2O solutions, respectively. All the other complexes were prepared by solid powder as described next.

Sample preparation

Free ligand solutions ([L1-L5]) (Figure **3.5**) were prepared from stock solutions of the ligands and dissolved with MilliQ water. The complexation procedure was optimized for this kind of systems, taking into account the complexation kinetics of lanthanide ions by macrocyclic ligands. For Ln^{3+} complexes the corresponding chloride salts were added to free ligand solutions in amounts corresponding to a 5% molar excess of ligand the resulting solution was heated under stirring for at least 12h. The value of pH was controlled by addition of stock HCl and NaOH solutions. The presence of free Ln^{3+} ions in solution was checked with the Xylenol Orange Test.[35] The resulting solutions used for ^1H NMR studies were evaporated under reduced pressure, re-dissolved in 1 mL of 99.9% D2O. In the case of Gd^{3+}-L1 and L3 complexes solution, the solution were lyophilized and re-dissolved in distillated water. The resulting solutions were then used to prepare the varying concentration solutions used in relaxometric studies.

^{1}H NMR

1D and 2D COSY ^{1}H NMR spectra were obtained at 298 and 333K for ligands L1 to L5 and its Ln^{3+} complexes in a Varian VNMRS 600 MHz NMR spectrometer operating at 599.72 MHz (^{1}H) with a 3-mm PFG triple resonance I.D. probe. For ^{1}H NMR experiments, solvent (D_2O) signal was used as an internal reference (^{1}H, δ 4.65 ppm). Spectra analysis and processing were performed with MestreNova (v6.0.2-5475, 2009 Mestrelab Research S.L.) software for both types of systems.

Relaxometric studies

Longitudinal relaxation studies were performed on a Bruker Minispec mq20 (20 MHz, B_0 = 0.47 T) relaxometer with a Haake DC10 (Thermo Electron Corporation) temperature controller, using the inversion-recuperation method (20 measurements, 4 scans). For determination of the longitudinal relaxivity (r_1) of Gd^{3+}-L1, R_{1p} values of 0-2 mM samples prepared from an initial 2 mM Gd^{3+}-L1 solution were determined at 298 and 310K. For Gd^{3+}-L3, the R_{1p} values of 0-5 mM samples prepared form an initial 5mM Gd^{3+}-L3 were also determined at 298K and 310K. The diamagnetic contribution R_{1dia} was obtained by measuring the R_{1obs} value of distilled water.

Temperature-dependence studies were performed with a 1 mM, pH ~7.0 Gd^{3+}-L1 and Gd^{3+}-L3 solution in the 275-350K range.

Data analysis

Data from relaxometric studies were processed with recourse to MS Excel 2010 v 14.0.7120.5000.

Preparation of the QDs

The QDs were synthetized in aqueous medium with adaptions of the previously described method by Santos. The QDs were then characterized by absorption and emission spectroscopy, utilizing a UV-Vis 1800 (*Shimadzu)* spectrophotometer and a LS 55 (*Perkin Elmer*) spectrofluorometer, respectively. The emission spectra were recorded by excitation at 365 nm.

Conjugation of the QDs and Transferrin

After the synthesis of the QDs they were diluted and the pH adjustment was made. EDC and Sulfo-NHS were used as coupling agents. For each 2mL of QDs was added 1mL of EDC and 1mL of Sulfo-NHS, and afterwards also added 92 µL of transferrin (Tf) and 184 µL of Tf. It was estimated that we have 1 molecule of Tf for 1 QD and 2 molecules of Tf for 1 QD with the amounts mentioned above.

The conjugation was then monitored by fluorescence microplate assay (FMA).

CHAPTER 3

Ln complexes analogues of DOTA: structural and relaxometric studies

3.1-Introduction

The design of new Gd^{3+}-based CAs is a very challenging process that needs a rational and systematic approach to obtain optimized results. As seen earlier the efficiency of a contrast agent can be described, its relaxivity (r_i). Relaxivity is governed by several parameters that need to be taken into account in order to obtain a more efficient CAs. The number of coordinated water molecules (q), the residence time of coordinated water molecules (τ_M), the second-sphere contribution (q_{ss} and τ_{Mss}) and the rotation correlation time (τ_R). All these parameters can be modulated by structural modification in the ligand backbone.

One of the most well-known and studied chelators is DOTA. The DOTA ligand (1,4,7,10-tetraazacyclododecane-1,4,7,10-tetraacetic acid) consists of a cyclen macrocycle with four acetate pendant arms bound to the four ring nitrogen atoms[36].(Figure 3.1)

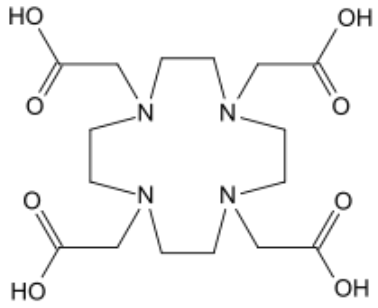

Figure 3.1- Chemical structure of the DOTA ligand.

The high thermodynamic stability and kinetic inertness presented by the Ln^{3+} complexes of this compound are the result of a good match between the size of the metal Ln ions and the macrocycle cavity.[13] The eight coordination sites of the central ion are occupied by four nitrogen atoms from the macrocycle and four oxygen atoms from the pendant arms. One coordination site is left for water molecule coordination. These two sets of coordination atoms form two planar and parallel planes, N_4 and O_4,

with the central metal ion between the two. The result is the presence of two diastereoisomers, Twisted square antiprismatic (TSAP) and Square antiprismatic (SAP). In DOTA-like complexes they are present in different abundances due to their different stabilities. The SAP isomer is present in higher abundance than the TSAP isomer and for this reason they are also denoted **M** (from Major) or **m** (from minor) isomers, respectively.[37] However, in Ln^{3+} complexes of DOTA derivatives the SAP/TSAP ratio can vary, depending on many factors.

Another important structural parameter is the opening angle ψ (O-Ln-O angle between transannular oxygen atoms), which is dependent on the distance between N_4 and O4 planes and the central ion radius (and consequently in the type of isomer). A relationship between the ψ angle and the number of bound water molecules (q) has been shown: If the angle is smaller than 135° no water molecule is coordinated to the central ion; if it is bigger than 145° the water molecule can be substituted for another group, such as a carboxylate group.[38]

The residence time (τ_M) of the water molecule in the first coordination sphere if the Ln complex is one of the most relevant parameters governing relaxivity and is closely linked with the two structural parameters mentioned above, mainly by steric crowding around the water binding site.

In general, TSAP isomers exhibit faster water-exchanging regimes due to higher steric crowding that favors water exchange. Although, due to the fact that the distance between the bound molecule and the metallic center is larger for TSAP isomers, the exchange of magnetic information is less effective. Consequently, the design of new CA is predominantly focused on the development of systems that have predominant SAP conformation.

So, fine modulation of the structural parameters are needed. Based on cyclen, three main types of modifications can be performed: i) modification at the macrocycle ring, introducing differences in cavity size and shape; ii) pendant arm removal; iii) modification at the level of the pendant arms, such as group substitution, arm elongation, introduction of linkers, spacers, targeting moieties or reactive function for further functionalization.[39]

A good example of a fine modulation was presented by Polásek and its colleagues, who achieved the adoption of an exclusive isomer by the Ln^{3+} complexes along the series. To obtain these results, a substitution of one acetate pendant arm of DOTA was performed with the introduction of a 2-methyl-pyridine-N-oxide one. The resulting ligand was named DO3A-py^{NO} (H3do3apyNO = 10-[(1-oxidopyridin-2-yl)methyl]-1,4,7,10- tetraazacyclododecane-1,4,7-triacetic acid) (**L6**) (Figure 3.2).

They also reported another ligand based on DOTA, DO3A-py^{NO-C} (H_4do3apy^{NO-C} = 10-[(4-carboxy-1-oxidopyridin-2-yl) methyl]-1,4,7,10-tetraazacyclododecane-1,4,7-triacetic acid), where the position 4 of the pyridine-*N*-oxide ring was functionalized with a carboxylic moiety. (**L7**) (Figure 3.2)

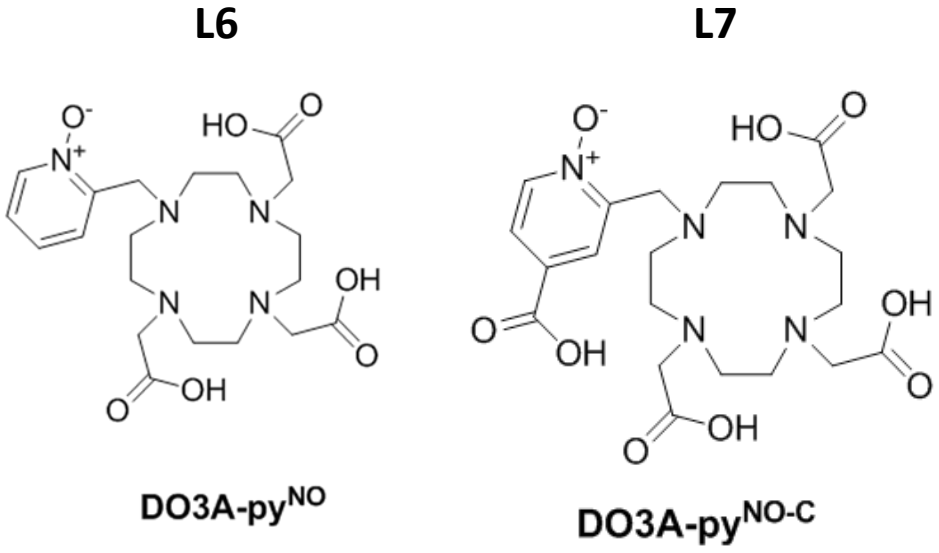

Figure 3.2- Chemical structure of DO3A-py^{NO} (**L6**) and DO3A-py^{NO-C} (**L7**).

Both complexes showed very similar structural properties, which favored the coordination of the pyridine-N-oxide oxygen atom to the central Ln^{3+} ion and forms a six-membered chelate ring instead of the most common five-membered one, which often prevails among the DOTA-like and DTPA-like complexes. This lead to a strong destabilization of the TSAP arrangement. The coordination of the pyridine-N-oxide arm

also lead to an enlargement of the ligand cavity in relation to the DOTA analogues, which result in greater flexibility of the coordination cage. This flexibility in combination with the higher steric hindrances led the authors to propose them as the main reasons for the observed fast water exchange rates (τ_M = 39 ns and 34 ns for DO3A-py^{NO} and DO3A-py^{NO-C}, respectively). These compounds also showed favorable properties for MRI applications, such as relaxivity values and thermodynamic stability similar to those used in clinical applications. [40–42]

Another possible approach was tried by Keizers *et al.* where the pyridine-*N*-oxide derivative was further modified with the objective of creating a caged lanthanide NMR probe, CLaNP-5 (Figure 3.3), to be attached to proteins for NMR structural studies. An additional pyridine-*N*-oxide arm was added in a *trans* position together with two 2-(amino- ethyl)methanethiosulfonate moieties in opposite acetate pendant arms, so that the respective Ln^{3+} complexes would have a 2-fold rotational axis (C_2 symmetry) with reduced ring and side chain isomerization and also with the capacity to be attached to close cysteine residues to reduce mobility of the complex moiety once conjugated to a peptide chain.[43]

Other relevant report was produced by Ubbink, who created a new lanthanide-chelating NMR probe, Caged Lanthanide NMR Probe-7 (CLaNP-7) (Figure 3.3). This chelator overcomes a major drawback of the total charge of the probe, which is 3+ after chelation for CLaNP-5. The new CLaNP-7 has only a 1+ total charge reducing the change in protein surface potential after probe attachment. [44]

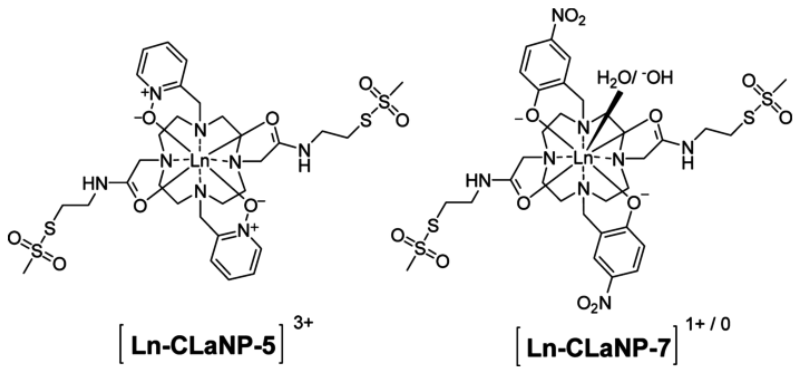

Figure 3.3- Structures of Ln-CLaNP-5 and Ln-CLaNP-7. Adapted from [44]

Finally it was reported the study of the mother of CLaNP-5, DO2A-*trans*-(py^{NO})$_2$ (4,10-bis[(1-oxidopyridin-2-yl)methyl]-1,4,7,10-tetraazacyclododecane-1,7-diacetic acid) (**L2**). (Figure 3.4) It was indicated that they tend to adopt an anti-Δ(λλλλ), anti-square antiprismatic (anti-SAP), conformation in aqueous solution. The report also revealed that this complex also have interesting relaxometric properties that are suitable for biological application. *

L2

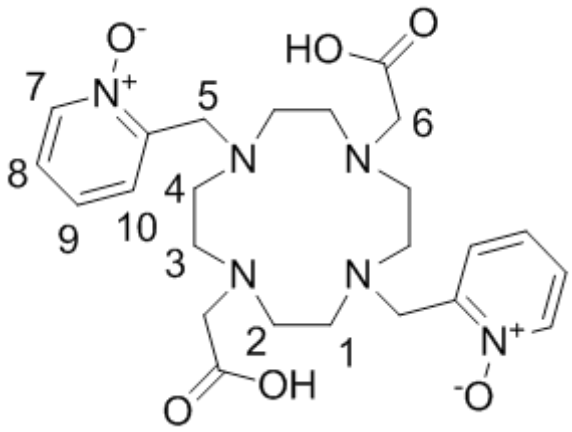

Figure 3.4- Chemical structure of DO2A-*trans*-(py^{NO})$_2$ (**L2**)

This study is focused on the Ln^{3+} complexes of four analogues of the bis(pyridine-N-oxide), DO2A-*trans*-(py^{NO})$_2$, analogue of DOTA. These ligands complexes are presented in Figure 3.5. It is intended to have more insights on the physico-chemical and structural dynamics properties of the complexes. To achieve that, a combination of the previous results with relaxometric and structural experiments was done, and a comparison with the results on Ln**L2** was undertaken.[45]

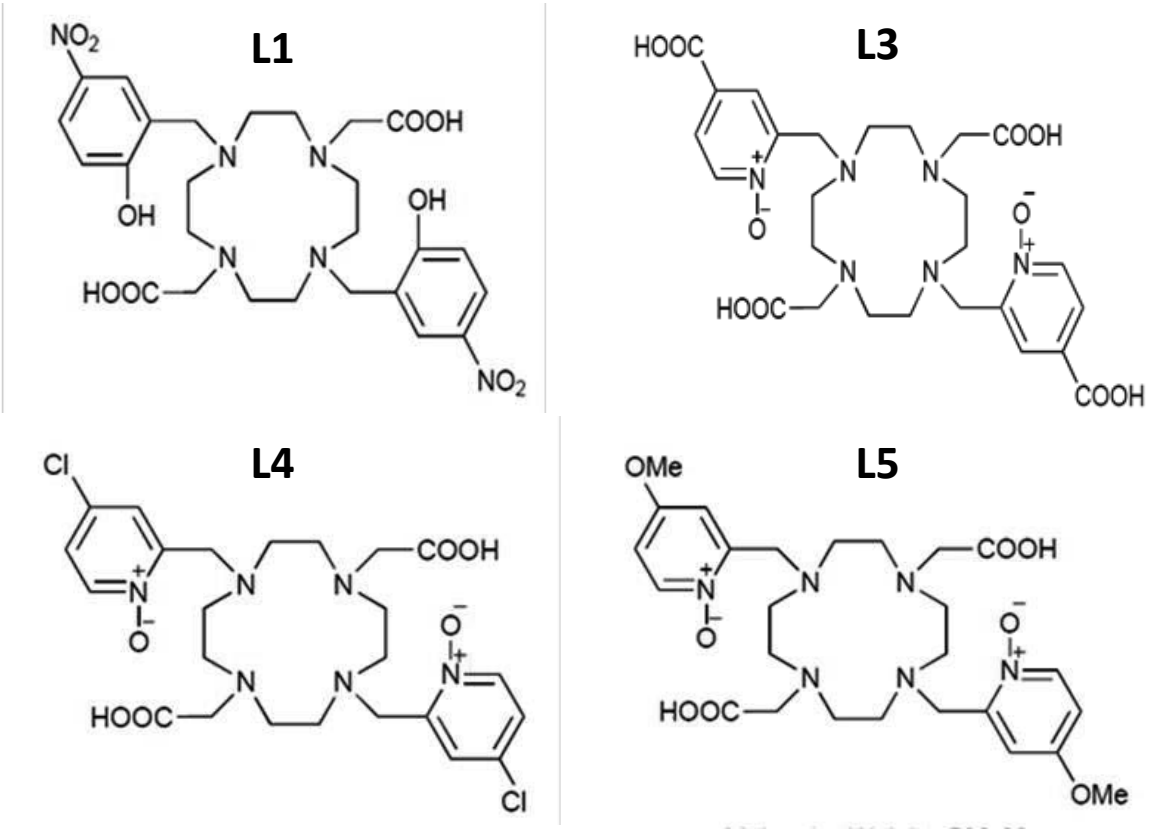

Figure 3.5- Ligands discussed in this work.

3.2-Results and Discussion

Relaxometric studies

The suitability of the Gd^{3+} complexes of the ligands **L1** and **L3** was evaluated by relaxometric studies, by determining their longitudinal relaxivity at different temperatures and compared with these of Gd-**L2**, Gd-**L6** and Gd-**L7**. The longitudinal relaxation times of Gd^{3+}-**L1** and **L3** solutions of increasing concentrations ranging from 0 to 2 mM for **L1** and from 0 to 5 mM for **L3** at pH ~7 were measured in order to obtain the correspondent r_1 value. (Figures 3.6 and 3.7)

The value of the relaxivity can be obtained as described in equation 3.1.

$$R_{1p} = R_{1obs} - R_{1dia} = r_1.[GdL] \qquad (3.1)$$

To acquire this value we did a plot of R_{1p} vs [GdL] and the r_1 value was 2.26 $mM^{-1}s^{-1}$ at 298 K and 1.95 $mM^{-1}s^{-1}$ at 310K for Gd-**L1** and 7.95 $mM^{-1}s^{-1}$ at 298 K and 6.46 $mM^{-1}s^{-1}$ at 310K for Gd-**L3**.

The obtained r_1 values for the Gd-**L1** are lower than those reported for Gd-DOTA (q=1, 4.2 $mM^{-1}s^{-1}$ at 298K and 3.5 $mM^{-1}s^{-1}$ at 310K).[38] These results were also compared with GL-L6 and Gd-L7, which have 4.04 $mM^{-1}s^{-1}$ and 4.54 $mM^{-1}s^{-1}$ respectively, at 310K. A first analysis can indicate that Gd-L1 probably has a q value lower than 1, when compared with other similar complexes. This is probably due to steric effects that disfavor the water binding in the first coordination sphere.

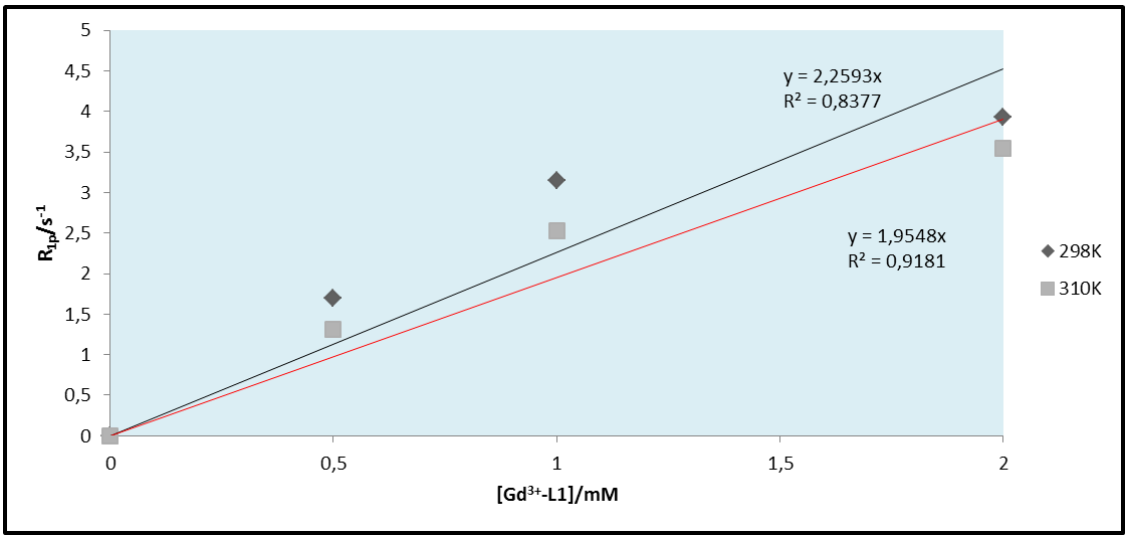

Figure 3.6- Paramagnetic longitudinal relaxation times (R_{1p}) as function of increased Gd^{3+}-L1 concentration at 298K and 310K. The linear trend lines obtained at both temperatures, are represented by a y=mx equation, where r_1=m.

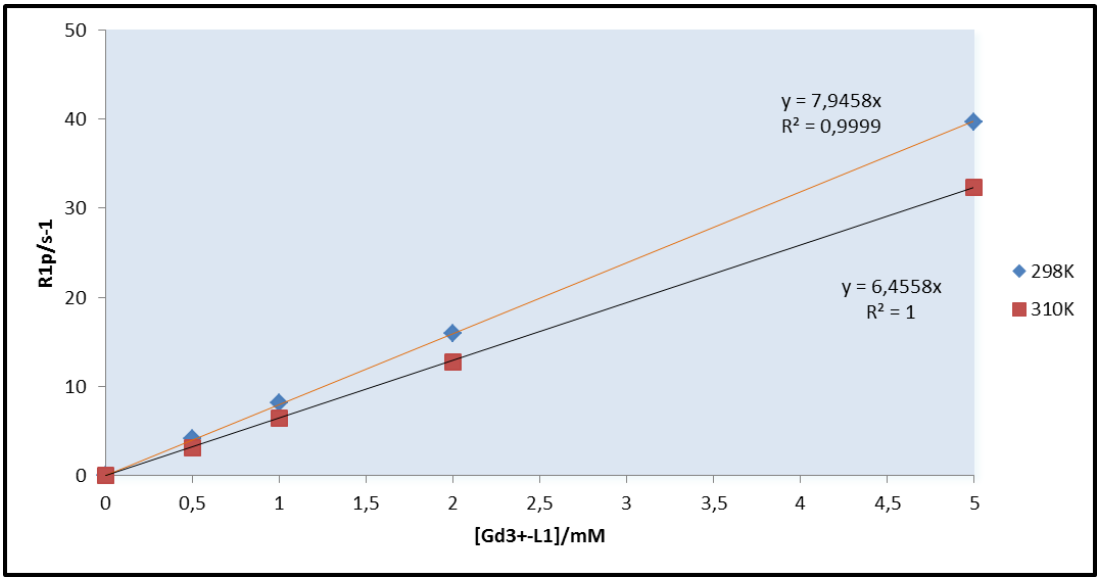

Figure 3.7- Paramagnetic longitudinal relaxation times (R_{1p}) as function of increased Gd^{3+}-L3 concentration at 298K() and 310K(). The linear trend lines obtained at both temperatures, are represented by a y=mx equation, where r_1=m.

Instead, the r_1 value of Gd-L3 at 298K and 310K indicates a value superior to those reported for DOTA and other commercially available compounds. They are also higher than those reported for the bis(pyridine-N-oxide) analogue Gd-**L2** (4.90 $mM^{-1}s^{-1}$ at 298K and 4.10 $mM^{-1}s^{-1}$ at 310K) which is structurally very similar. The results are contradictory which could indicate a different coordination pattern for the Gd^{3+} ion, and that could result in different crowding around the water coordination position. However, no direct measurement of the q value was performed to confirm these hypotheses. Therefore, more tests such as ^{17}O experiments are needed with the view to confirm and proceed with further analysis. These results could also mean that there is free Gd^{3+} but further results are needed to confirm this hypothesis.

Variable temperature studies were also performed with 1 mM Gd-L1 and Gd-L3 solutions at 20 MHz in the 275-350K temperature range. (Figures 3.8 and 3.9)

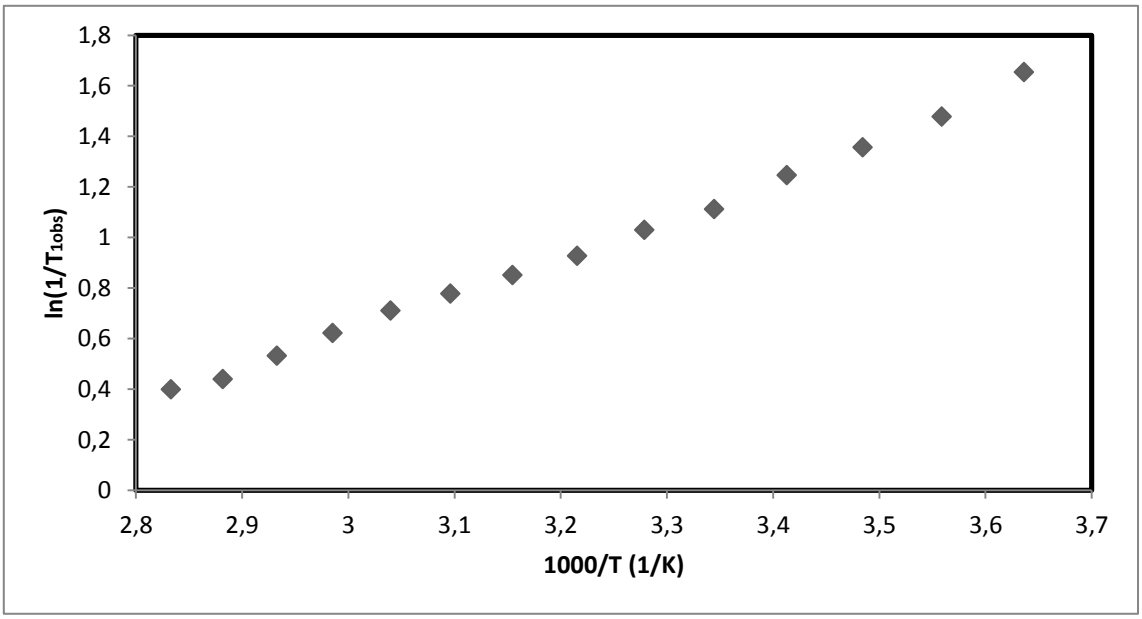

Figure 3.8- $\ln(1/(T_{1obs}))$ of a 1 mM Gd^{3+}-L1 solution as a function of temperature.

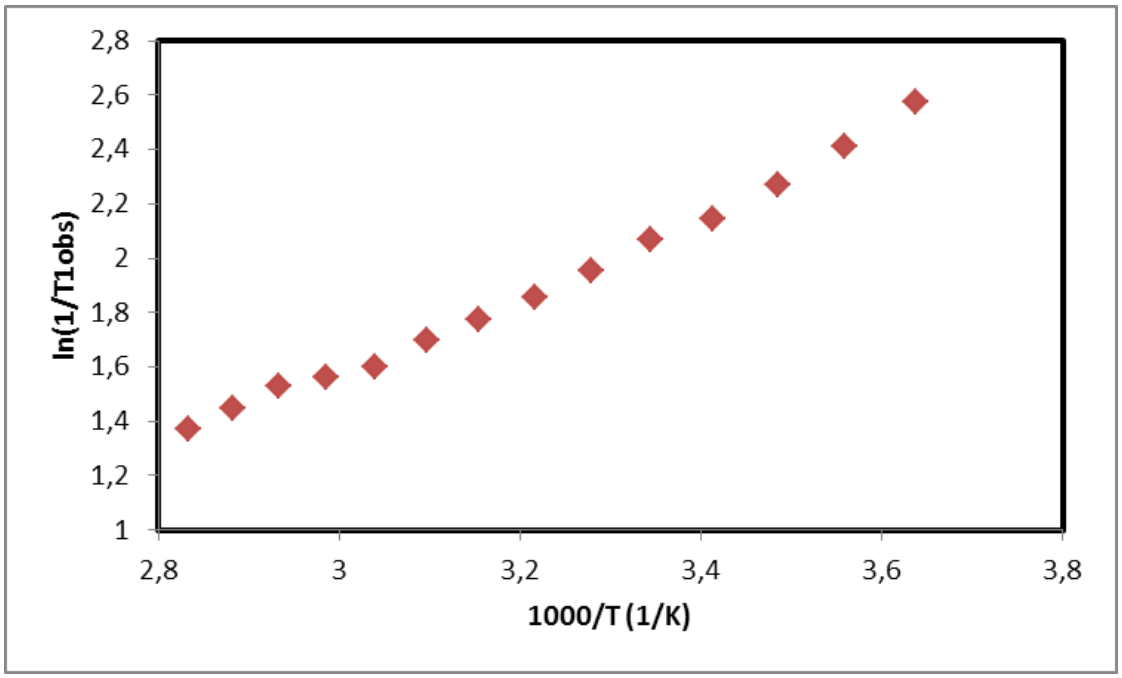

Figure 3.9- - ln(1/(T_{1obs})) of a 1 mM Gd^{3+}-L3 solution as a function of temperature.

The obtained profile indicates that the systems are in a fast exchange regime, given the positive slope of the curve. However, this cannot be considered a direct measure of the residence time of the water molecules. Only with simultaneous fitting of the curves obtained by VT-^{17}O NMR and ^{1}H NMRD, under the GSBM framework, could this parameter be determined.

These results suggests that the behavior of the Gd^{3+} complexes are in agreement with the previously described for Gd**L2**.[45] Even thought, more insights are need before advancing to toxicity tests. Thermodynamic and kinetic tests such as transmetallation or pH dependence or the magnetic field dependence studied by ^{1}H NMRD are needed to perform a real evaluation of the compounds.

Structural Studies

A structural elucidation of the Ln^{3+} complexes of all the five ligands was attempted by 1D ^{1}H NMR and 2D COSY ^{1}H NMR. All the 1D ^{1}H NMR spectra of the lanthanide series of the ligands was acquired at 298 K and 333K. At 333K significant line broadening and signal merger occurs, and therefore the acquisition of the NMR spectra at this temperature was abandoned since their assignment was found impossible. This could indicate that a dynamic processes occurring at this temperature range involving extended conformational interconversion.

In this study we compared the previously recorded spectra for the Ln^{3+} complexes L2, L6 and L7 with those of the four ligands in study and did a full study along the lanthanide series. Proton signal assignment was based on the 2D COSY ^{1}H NMR spectra and the comparison with previous published spectra of the complexes of bis(pyridine-N-oxide) (**L2**) DOTA analogue.[45]

The spectra collected for the **L4** ligand are presented Figures 3.10 and 3.11, whereas the results obtained for the **L5** ligand are shown at Figures 3.12 and 3.13.

Considering the spectrum of L4 at 298K, the axial and equatorial resonances of the ring ethylenic groups are present at 2.94 and 3.46 ppm. The methylenic protons of the pendant arms are present at 3.61 ppm for the pyridine pendant arm and at 4.0 ppm for the acetate pendant arm. The pyridine arm protons are present in a more shifted zone. H7, H8 and H10 correspond to 7.88, 7.50 and 8.22 ppm respectively.

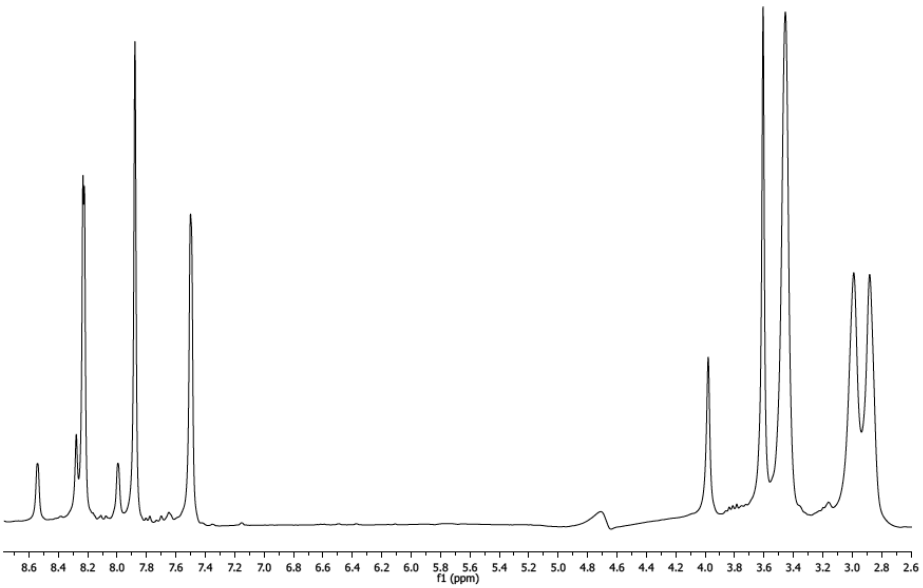

Figure 3.10- ^{1}H NMR spectrum of L4 solution at 298K.

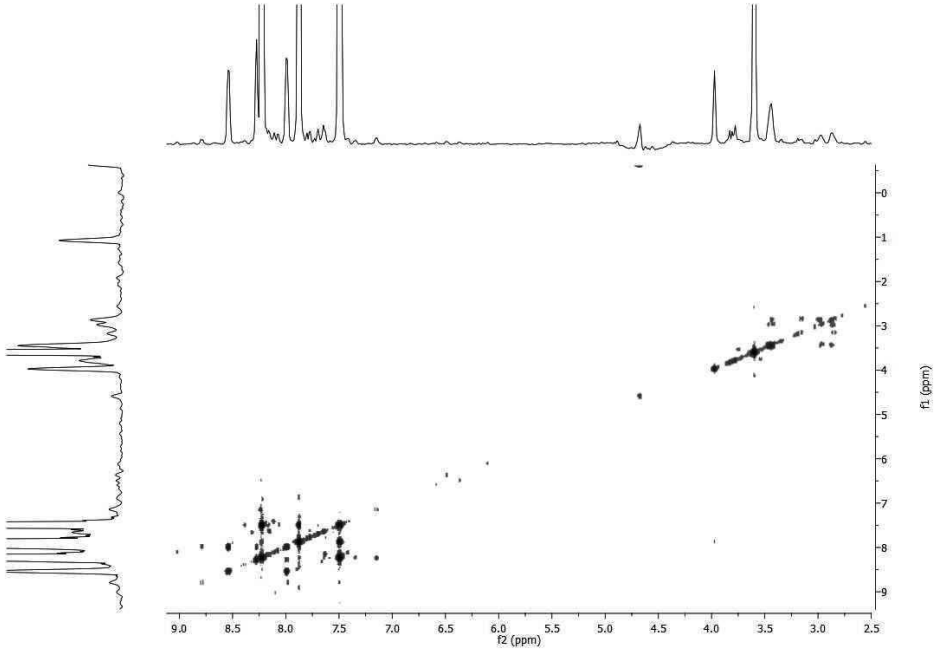

Figure 3.11- 2D COSY ^{1}H NMR spectrum of L4 solution at 298K

Like L4, the ligand L5 was studied by 1D and 2D ^{1}H NMR. Considering the 1D spectrum of L5 at 298K, the axial and equatorial resonances of the ring ehtylenic groups are present at 2.85 and 3.38 ppm. The methylenic protons of the pendant arms are present at 3.5 ppm for the pyridine pendant arm and at 3.98 ppm for the acetate pendant arm. The protons of the metil group of the pyridine are present at 3.88 ppm. The pyridine arm protons correspond to 6.98, 7.36 and 8.17 ppm and can be assigned to H8, H7 and H10 respectively.

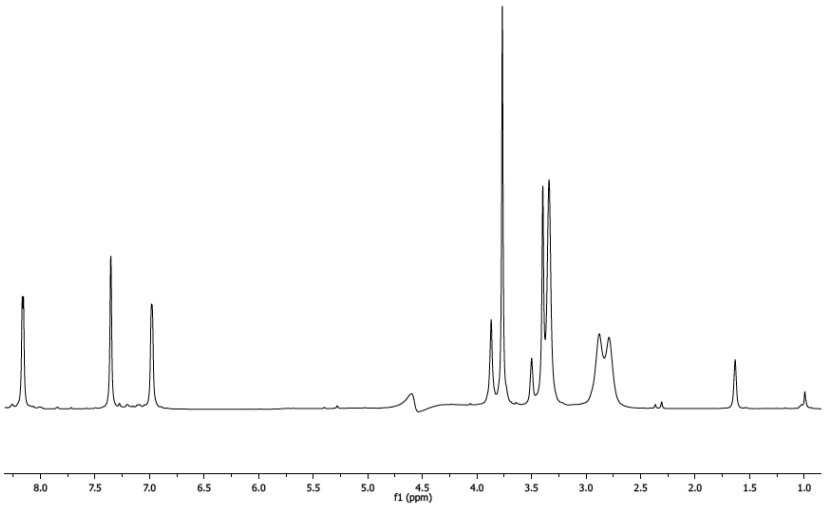

Figure 3.12- ^{1}H NMR spectrum of L5 solution at 298K.

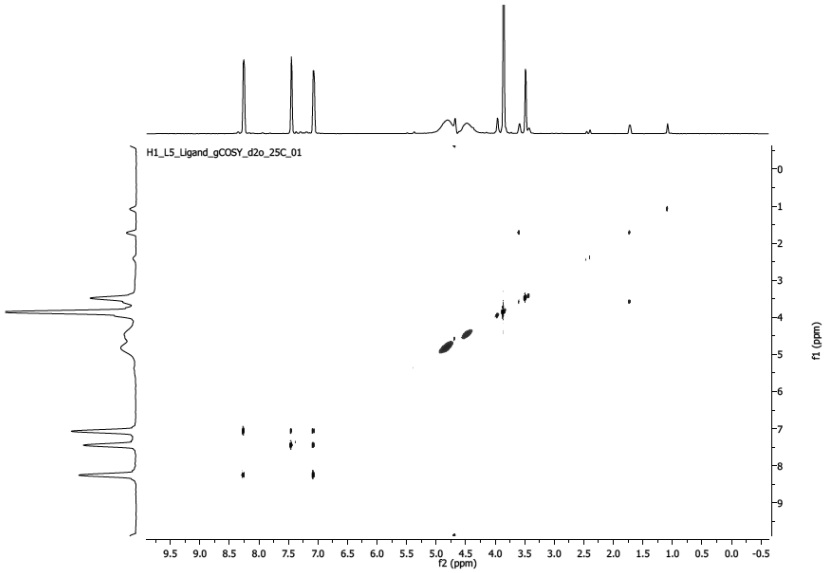

Figure 3.13- 2D COSY ^{1}H NMR spectrum of L5 solution at 298K.

To understand the coordination scheme of LnL, we studied the diamagnetic Lu^{3+} complexes. But, as seen in figure 3.14 the complete assignment is impossible, even with recourse to the 2D COSY also obtained. Even though the assignment of the methylpyridine-N-oxide was possible since these protons produce well defined peaks.

The results also suggest that all the macrocycle protons are involved in complex formation, since there is a shift for all their resonances and also from the methylenic protons of the pendant arms which also suggest that all the four arms are involved in metal coordination.

The Yb^{3+}L and spectra were also obtained (Figure 3.15). 2D- COSY experiments were also tried but no cross-peaks were detected, and for that reason the data are not presented here.

Based on previous reports with other similar complexes like CLaNP-5 and DO3A-py^{NO} Ln^{3+} complexes, a possible assignment was tried.

The spectra of all the four complexes in study also further suggest that only one isomer is present in solution at this temperature. Compared with the analogues aforementioned, the results suggest that based on the large shifts observed it is more likely to be the SAP isomer, which is in agreement with previously reported results.

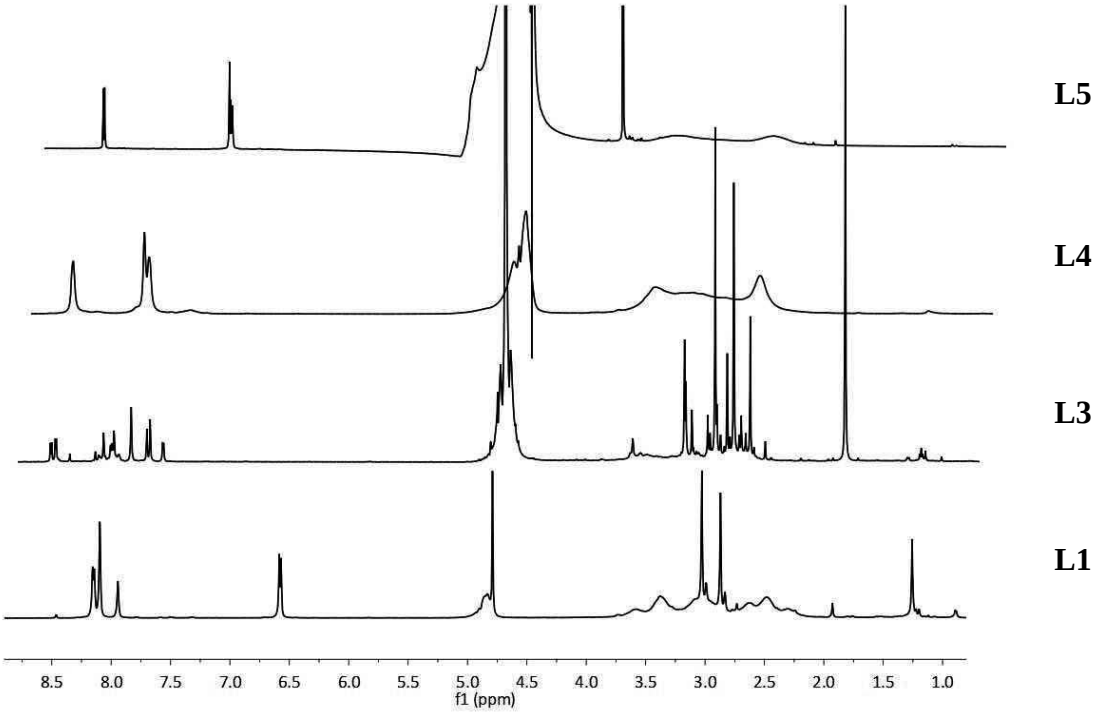

Figure 3.14- ^{1}H NMR spectrum of Lu-L complexes at 298K, L=L1, L3, L4 and L5.

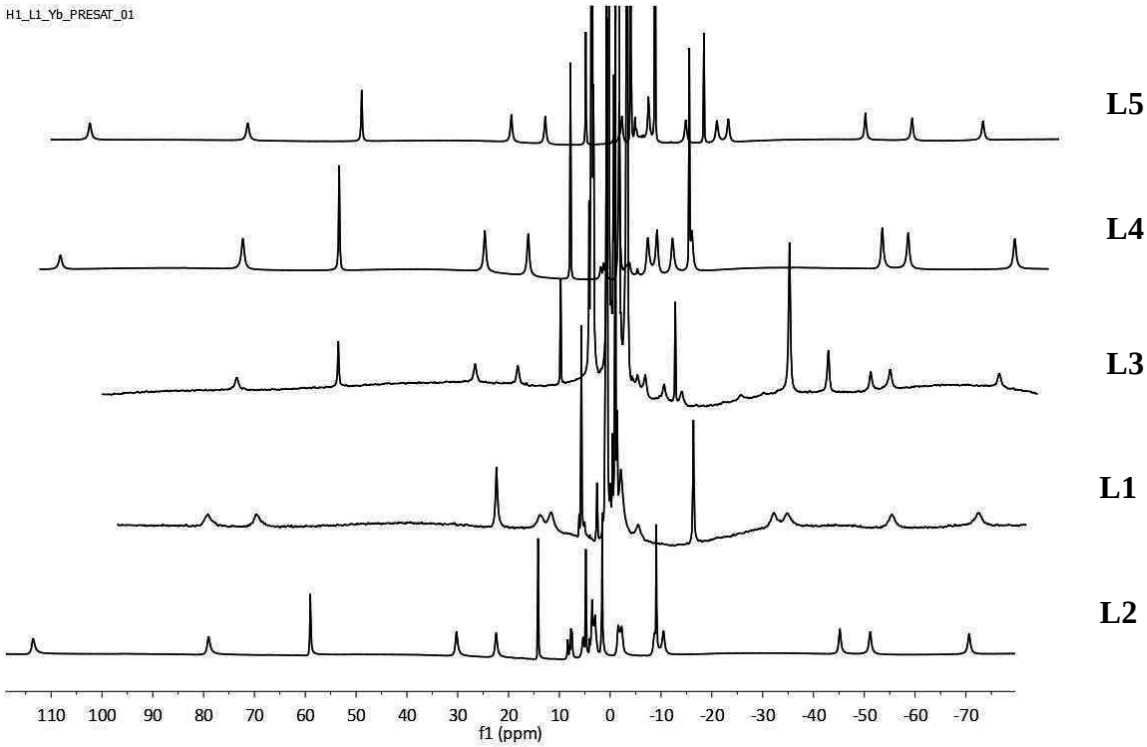

Figure 3.15- ^{1}H NMR spectra of Yb-L solutions at 298K. L= L2, L1, L3, L4 and L5.

Since the Yb^{3+} radius is very similar to the Lu^{3+} ion their structure should be very similar, and they can be combined in order to calculate the paramagnetic shifts of the only assigned protons, the ones from pyridine-N-oxide arms.

Tables 3.1 and 3.2 show the possible assignments of the pyridine protons as well as the paramagnetic shifts obtained.

Table 3.1- ^{1}H shifts (in ppm) for L4 solutions obtained experimentally.

	L4	**Lu^{3+}-L4**	**Yb^{3+}-L4**	**δ_i^{dia}**	**δ_i^{exp}**	**δ_i^{para}**
	δ (ppm)					
H7	7.88	7.80	60.02	0.08	52.14	52.22
H8	7.50	7.76	14.56	-0.26	7.06	6.8
H10	8.22	8.40	-9.02	-0.18	-17.24	-17.42

Table 3.2- ^{1}H shifts (in ppm) for L5 solutions obtained experimentally.

	L5	**Lu^{3+}-L5**	**Yb^{3+}-L5**	**δ_i^{dia}**	**δ_i^{exp}**	**δ_i^{para}**
	δ (ppm)					
H7	6.98	7.14	57.52	-0.16	50.54	50.38
H8	7.36	7.15	13.68	0.21	6.32	6.53
H10	8.17	8.21	-9.90	-0.04	-18.07	-18.11

For further characterization along the lanthanide series, it was also obtained the 1H NMR spectra of the Ln-L complexes with other Ln^{3+} ions. It was also tried to obtain the 2D NMR spectra of the complexes but no cross-peaks were observed for most of the complexes which made their assignment impossible to perform.

The results are present in Figures 3.16 to 3.25. These results will be used for in further studies to separate the contribution of the PCS and the Fermi Contact to the total shift by the Reilley protocol.

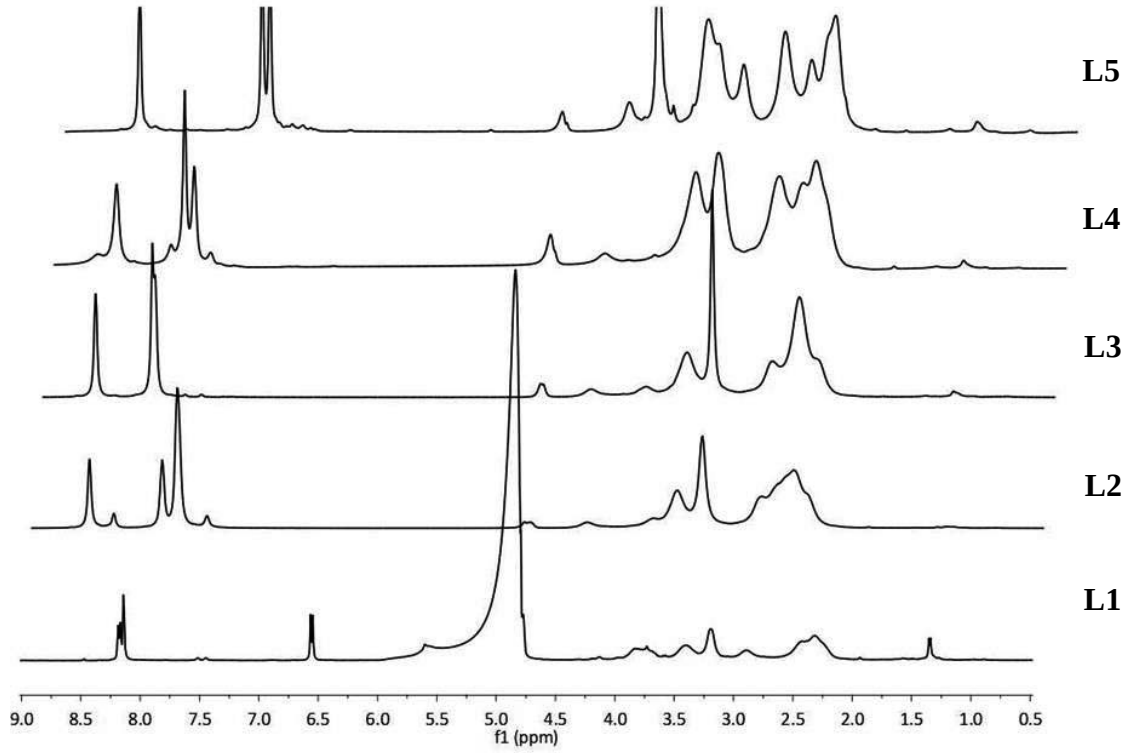

Figure 3.16- ^{1}H NMR spectrum of La-L complexes at 298K, L= L1, L2, L3, L4 and L5.

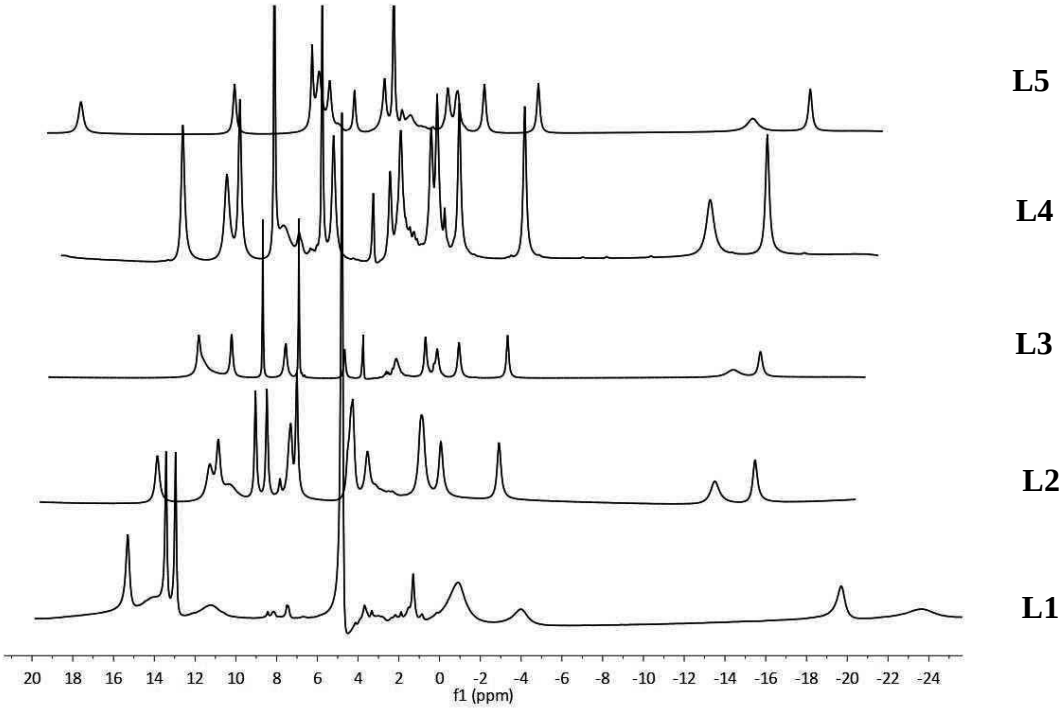

Figure 3.17- ^{1}H NMR spectrum of Ce-L complexes at 298K, L= L1, L2, L3, L4 and L5.

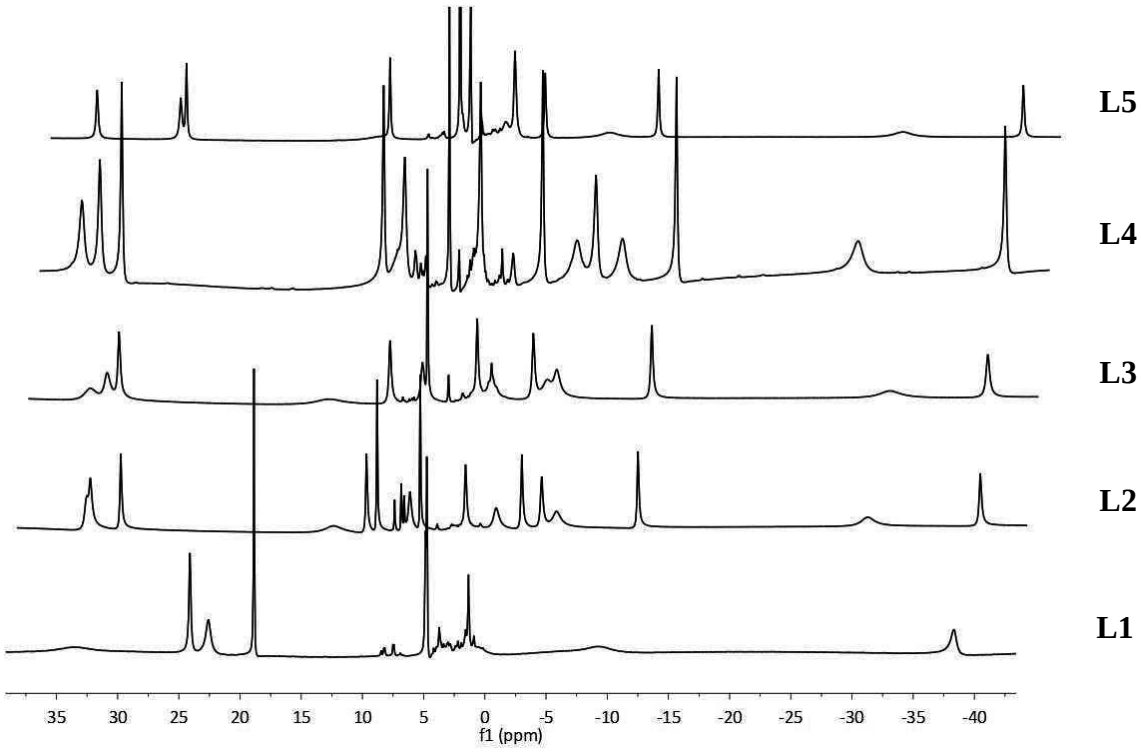

Figure 3.18- ^{1}H NMR spectrum of Pr-L complexes at 298K, L=L1, L2, L3, L4 and L5.

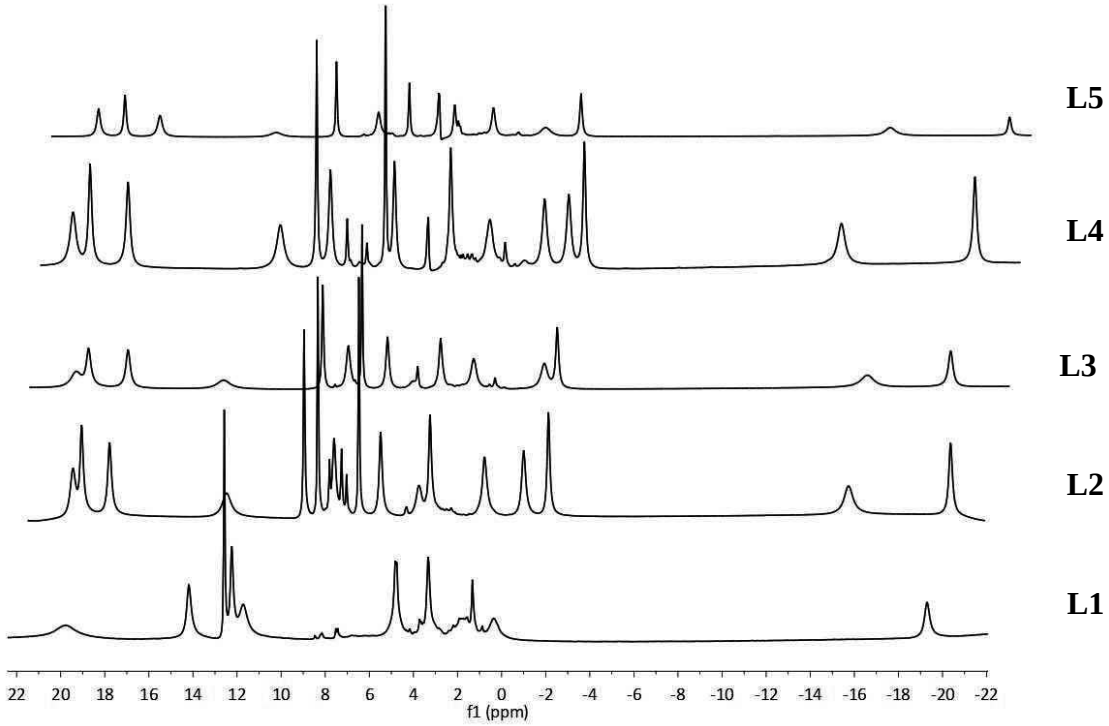

Figure 3.19- ^{1}H NMR spectrum of Nd-L complexes at 298K, L=L1, L2, L3, L4 and L5.

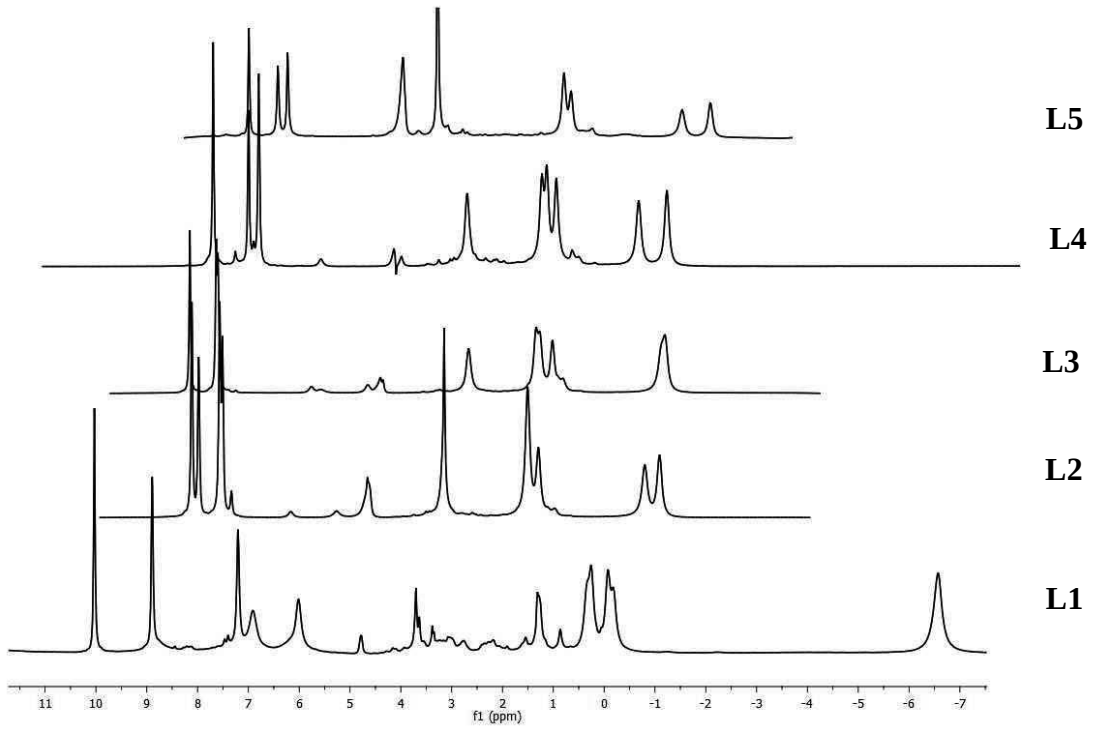

Figure 3.20- ^{1}H NMR spectrum of Sm-L complexes at 298K, L=L1, L2, L3, L4 and L5.

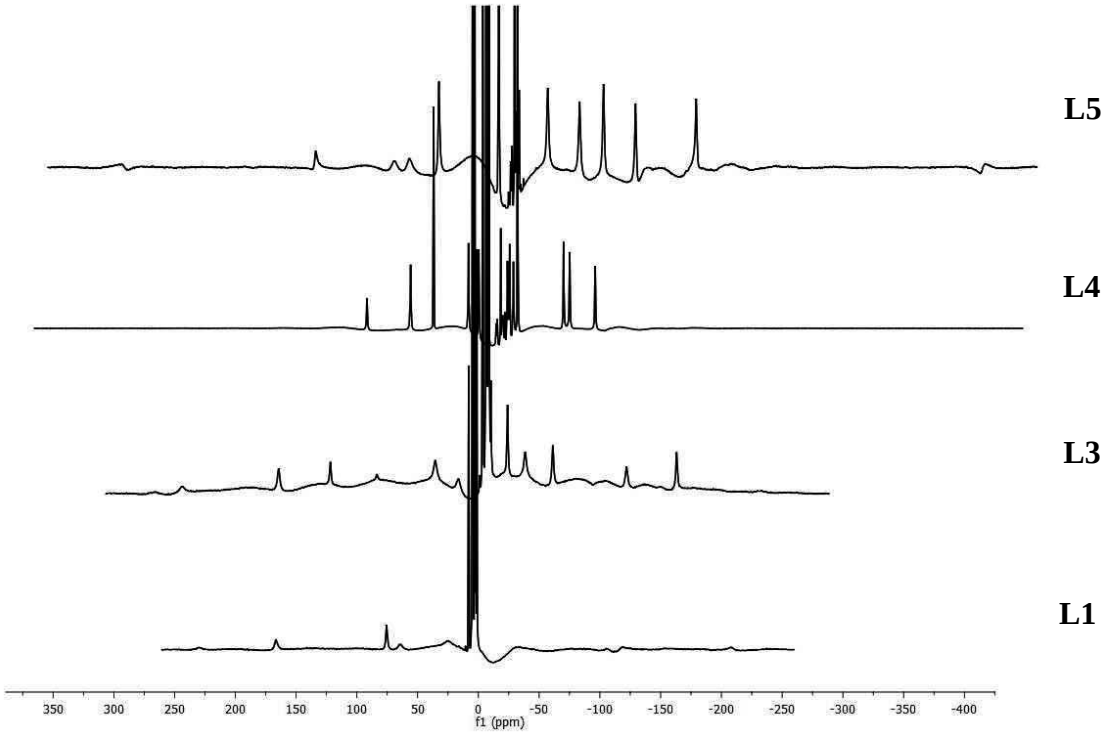

Figure 3.21- ^{1}H NMR spectrum of Tb-L complexes at 298K, L=L1, L3 L4 and L5.

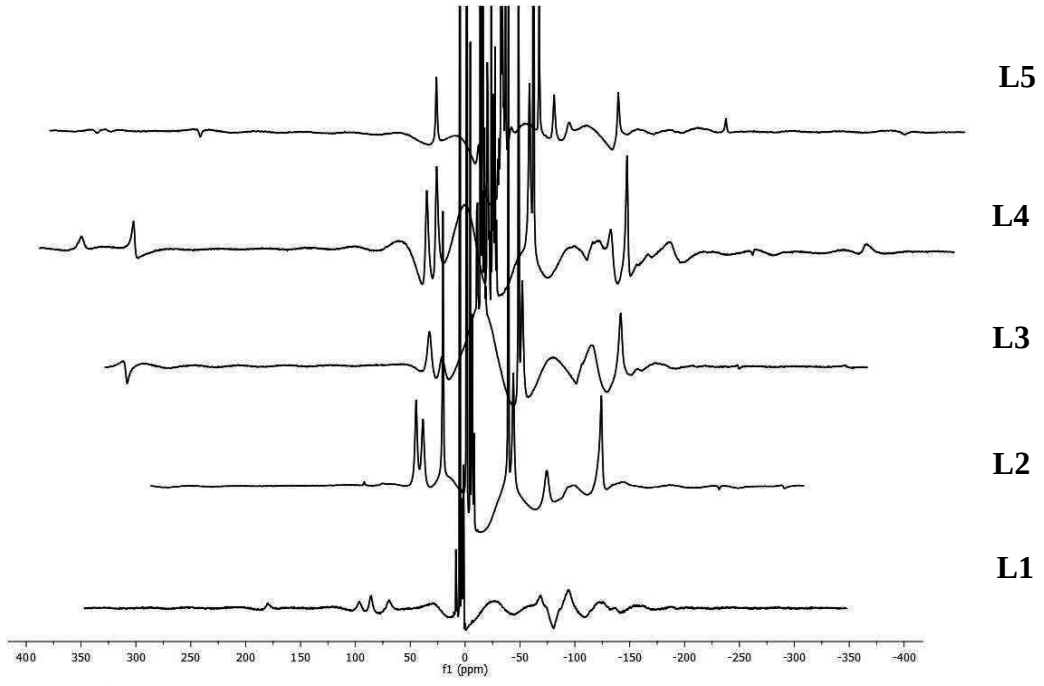

Figure 3.22- ^{1}H NMR spectrum of Dy-L complexes at 298K, L=L1, L2, L3, L4 and L5.

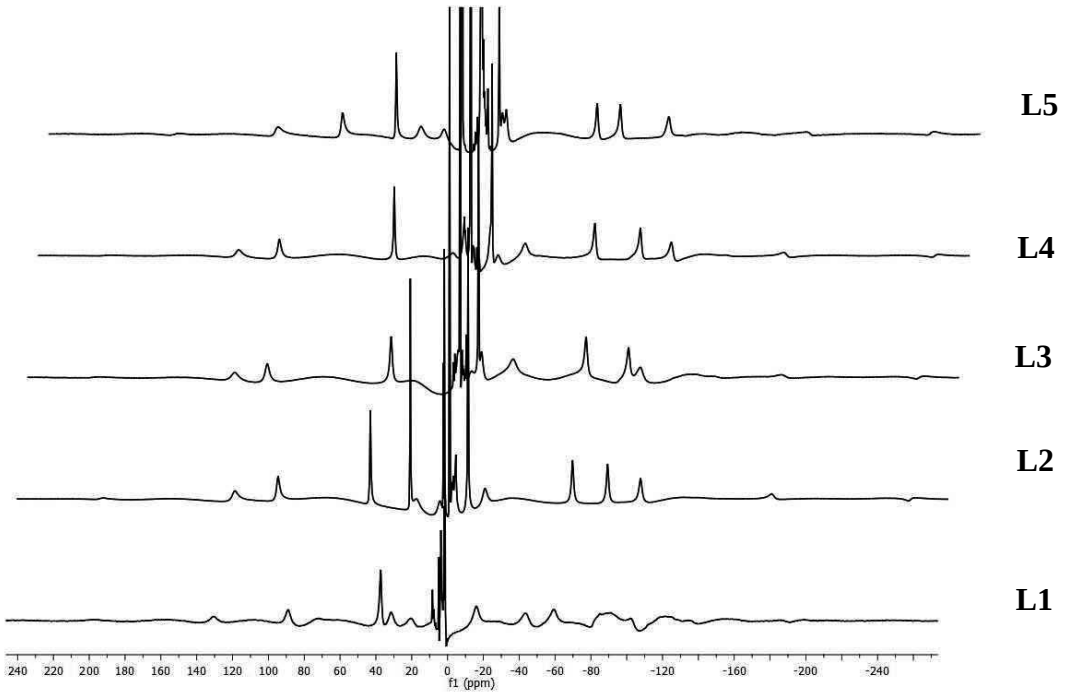

Figure 3.23- ^{1}H NMR spectrum of Ho-L complexes at 298K, L=L1, L2, L3, L4 and L5.

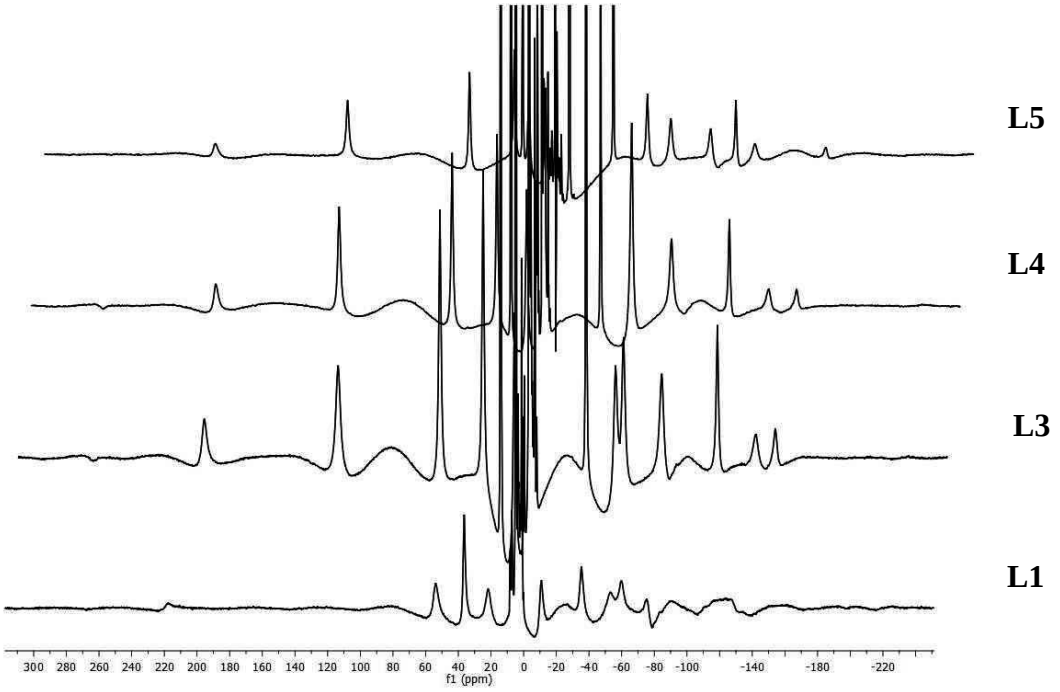

Figure 3.24- ^{1}H NMR spectrum of Er-L complexes at 298K, L=L1, L3, L4 and L5.

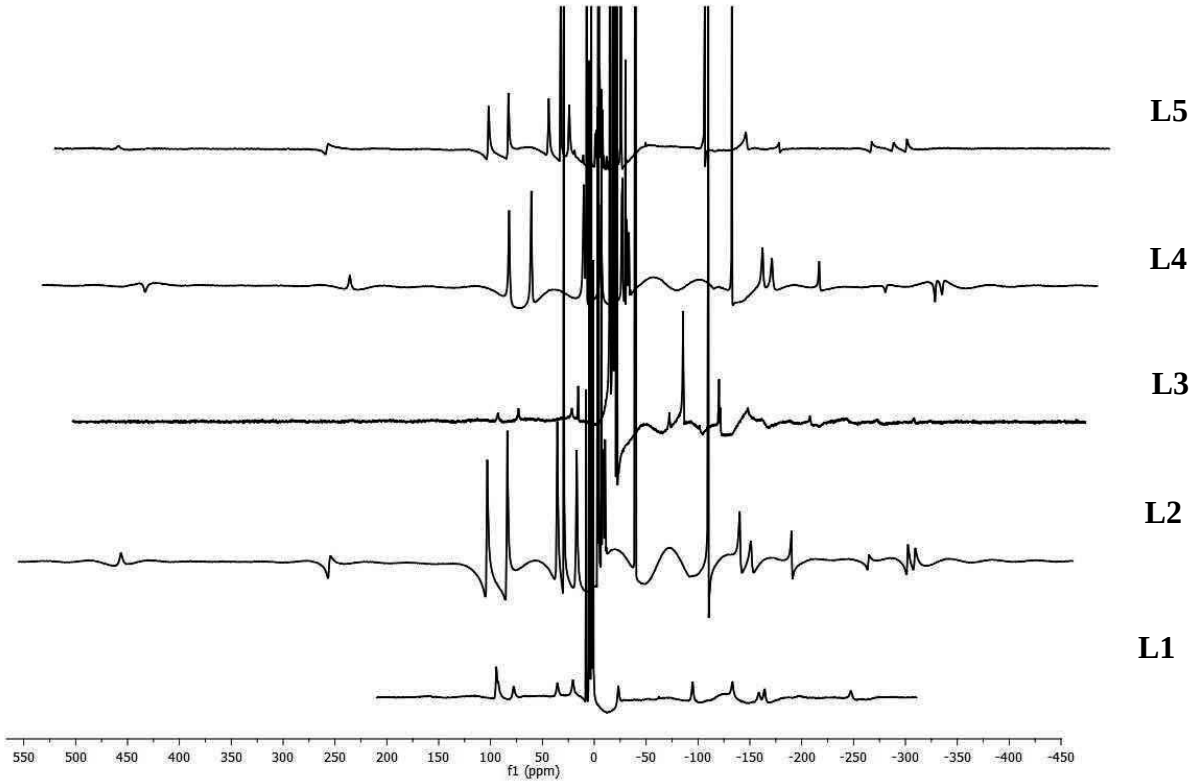

Figure 3.25- ^{1}H NMR spectrum of Tm-L complexes at 298K, L=L1, L2, L3, L4 and L5.

Despite the absence of any assignment, it is clear that for the first part of the series more than one isomer is present at this temperature. It is also clear that the previously studied L2 produces larger shifts than the other complexes, being followed by L4. L1 is the complex with less efficient shifts produced. This is mainly related to the different assymetries of their magnetic susceptibility tensors, which determine the values of the pseudo-contact shifts, although the contact contribution may also vary depending on the ligand electronic structures. The study or their relative contributions will be the object of future studies.

3.3-Conclusions

This work presents an improvement in the study of the bis(pyridine-N-oxide) analogues of DOTA. It is showed here that the relaxometric studies of the complexes L1 are in agreement with the previously reported results. In spite of the values obtained were lower than the clinically approved MRI CAs, the results showed a promising pathway for further studies.

It was also proved that these complexes have a behavior similar to the previously described L2, being present mainly in the SAP isomer for the second part of the lanthanide series. The results also showed that L2 produces the larger shifts being followed by L4. The less efficient complex is L1, with disparate results of the remaining three test compounds.

Nevertheless, a more complete study with recourse to different technologies, such as computational methods (eg. DFT calculations) and X-ray structure determinations, are needed for a better understanding of the results.

CHAPTER 4

QD doped with Gd^{3+}: a new class of Bimodal CAs

4.1-Introduction

Multimodal imaging has emerged as a possible way to improve the quality of the images acquired by a combination of imaging modalities. One of the most usual approaches is the combination of MRI and Optical imaging.

Several strategies of CA development have been applied in order to obtain the best results for a combination of different imaging modalities. A possible approach is the use of QDs as basis to create multimodal agents. Several examples have been reported in the literature and previously revised.[46,47]

A good way to create an efficient multimodal imaging agent, is to combine the great capacity of QDs as optical imaging agents with the use of Gd^{3+} as relaxation enhancement agents for MRI. There are several approaches know so far to achieve this combination, core/shell and heterostructures of magnetic materials and QDs, QDs doped with paramagnetic ions, composite nanostructures combining magnetic particles and QDs, and QDs with a paramagnetic coating of Gd-chelates.[48] Mulder evidenced that QDs can by coated with paramagnetic Gd^{3+} complexes[19], Archer and his colleagues showed that they can also be doped with Mn^{2+} ions[49] and Jin proved that they can by functionalized with Gd3+ chelates to obtain a bimodal probe.[50] Thus, the last two approaches were chosen as good ways to create this bimodal agent.

Another interesting feature of a QD is its capacity to be functionalized with a targeting agent. In this work, the QDs were conjugated with transferrin, a common biomarker for cancer.[51]

Therefore, in this chapter of the thesis it is aimed to obtain an efficient bimodal agent, which combines the great sensitivity of Optical Imaging with the great spatial resolution of MRI and with a great capacity to be specifically targeted to diseased cells.

4.2-Results and Discussion

Doping efficiency of the QDs CdTe

A reported problem to the construction of this type of complexes is that these nanosystems host matrix have a tendency to remove all the impurities from their surface in a process of "self-purification", which may compromise the construction of this QDs doped with Gd^{3+}. [52]

Therefore it is crucial to understand if there is an efficient production of these complexes. These were assigned with the use of Inductively Coupled Plasma Optical Emission Spectrometry (ICP-OES) and the results are depicted in table 4.1.

Table 4.2: Quantification of the metallic ion concentration of Cd^{2+} and Gd^{3+} present in the QDs of CdTe by ICP-OES.

Sample	$[Cd^{2+}]$ (mg/L)	$[Gd^{3+}]$ (mg/L)	$[Gd^{3+}]$ (mM)
CdTe	980,8	<0,5	0
CdTe:Gd (1)	1.111	236,8	1,51
CdTe:Gd (2)	809	240,3	1,53
CdTe:Gd (3)	1.275	236,4	1,50

According to the date of ICP-OES about 75,7% of the Gd^{3+} ions added were present after washes. This shows that this dopping process can be considered efficient and a viable alternative to create a bimodal contrast agent.

Relaxometric Studies

The newly formed complexes were then studied by relaxometric methods, to check if they were suitable for use as MRI CAs.

The relaxation times of the complexes were acquired at 20 MHz and 298K. The results are summarized at Table 4.2.

Table 4.2: T_1 and T_2 relaxation times of the CdTe solutions at 20MHz and 298K.

Samples	$T_{1(obs)}$ **(s)**	r_1 $(s^{-1}mM^{-1})$*	$T_{2(obs)}$ **(s)**	r_2 $(s^{-1}mM^{-1})$*
CdTe:Gd not washed	1,180	2.07	0,953	3.01
CdTe:Gd, washed	0,325	12,2	0,283	14,2
CdTe:Gd, washed	0,190	22,1	0,162	26,2

*The diamagnetic contribution was considered the solution of CdTe without any Gd^{3+} ion.

As seen from the results it is clear that T_1 and T_2 values significantly decreased with the wash, corresponding to an increase in their relaxivity. This can correspond to coordination with the stabilizing agent of the particle by the Gd^{3+} ions, which is not the result we were expecting. Even though, the results are an interesting preliminary data to a more complete and integrated result.

Confirmation of the Bio-conjugation of the Transferrin and the QDs

A possible way to check the conjugation of a bio-molecule with a fluorescent compound is with recourse to a microplate reader.[53]

This technique is based on the affinity of the plaque, of polystyrene, with the protein. In this way, only the QDs conjugated with the protein give a fluorescent signal, and this signal is more intense if more QDs are conjugated with the biomolecule. The calculation of the relative increase in fluorescence (F_i) is given by Equation 4.1.

$$F_i\% = \frac{(F_{Bio} - F_{Control})}{F_{Control}} \times 100\% \qquad (4.1)$$

Where F_{bio} is the fluorescence of the bio-conjugate and $F_{control}$ is the fluorescence of the control. Table 4.2 presents the results of the conjugation with transferrin.

Table 4.3-Results of the fluorescence microplate reading. F_i%- increase in fluorescence.

	Conjugate Day 1	**Conjugate Day 4**	**Conjugate Day 12**	**Conjugate Day 15**	**Conjugate Day 21**
Systems			Fi%		
Conjugate 1Tf:1QDs	**4813**	**7440**	**8652**	**2584**	**247**
Conjugate 2Tf:1QDs	**7173**	**15264**	**18106**	**20203**	**9315**

As seen in table 4.3 it is possible to obtain an efficient conjugation between the QDs and Transferrin, and this covalent conjugation is more efficient if two molecules of transferrin are conjugated with one QD. The results also show a good stability of the complex formed since only after 12 days the fluorescence starts to decrease.

4.3-Conclusions

The results present in this chapter are the preliminary studies of an integrated cooperation project that aims to develop efficient bimodal CAs with the combination of QDs and lanthanide complexes.

The results indicate that the doping strategy may not be the most effective, since the Gd^{3+} ions are coordinating with the coupling agent and not doping the surface of the particle. Even though, the results are an interesting first data for a more complete strategy. It is planned that these QDs can be combined with lanthanide complexes previously studied, creating in this way an efficient bimodal CA.

These results also suggest that is possible to conjugate these nanosystems with Transferrin. This conjugation is more efficient if there is more than one molecule of Transferrin is covalently link with the QDs, and it was also proved that this systems are quite stable since that only after 12 days the complexes started to lose fluorescence.

References

1. Fricker, S. P. The therapeutic application of lanthanides. *Chem. Soc. Rev.* **35,** 524–33 (2006).

2. Evans, C. H. Interesting and useful biochemical properties of lanthanides. *Trends in Biochemical Sciences* **1976,** 1–5 (1983).

3. Sherry, A D., Caravan, P. & Lenkinski, R. E. Primer on gadolinium chemistry. *J. Magn. Reson. Imaging* **30,** 1240–8 (2009).

4. Hinckley, C. Paramagnetic shifts in solutions of cholesterol and the dipyridine adduct of trisdipivalomethanatoeuropium (III). A shift reagent. *J. Am. Chem. Soc.* **1085,** 5160–5162 (1969).

5. Keizers, P. H. J. & Ubbink, M. Paramagnetic tagging for protein structure and dynamics analysis. *Prog. Nucl. Magn. Reson. Spectrosc.* **58,** 88–96 (2011).

6. Liu, W.-M., Overhand, M. & Ubbink, M. The application of paramagnetic lanthanoid ions in NMR spectroscopy on proteins. *Coord. Chem. Rev.* **273-274,** 2–12 (2014).

7. Geraldes, C. F. in *Rare Earth Elem.* **227,** 43–78 (2012).

8. Pintacuda, G., John, M., Su, X.-C. & Otting, G. NMR structure determination of protein-ligand complexes by lanthanide labeling. *Acc. Chem. Res.* **40,** 206–12 (2007).

9. Bertini, I. *et al.* The catalytic domain of MMP-1 studied through tagged lanthanides. *FEBS Lett.* **586,** 557–67 (2012).

10. Weissleder, R. Molecular Imaging. *Radiology* **219,** (2001).

11. Damadian, R. Tumor detection by nuclear magnetic resonance. *Science* **171,** 1151–1153 (1971).

12. Lauterbur, P. C. Image Formation by Induced Local Interactions: Examples Employing Nuclear Magnetic Resonance. *Nature* **242,** 190–191 (1973).

13. Merbach, A. E.; Toth, E. *The Chemistry of Contrast Agents in Medical Magnetic Resonance Imaging.* (John Wiley&Sons, 2001).

14. Laurent, S., Elst, L. Vander & Muller, R. Lanthanide complexes for magnetic resonance and optical molecular imaging. *Quarterly Journal of Nuclear Medicine and Molecular Imaging* **53,** 586–603 (2009).

15. Mendonça-Dias, M. H., Gaggelli, E. & Lauterbur, P. C. Paramagnetic contrast agents in nuclear magnetic resonance medical imaging. *Semin. Nucl. Med.* **13,** 364–376 (1983).

16. Geraldes, C. F. G. C. & Laurent, S. Classification and basic properties of contrast agents for magnetic resonance imaging. *Contrast Media Mol. Imaging* **4,** 1–23 (2009).

17. Frullano, L. & Meade, T. J. Multimodal MRI contrast agents. *J. Biol. Inorg. Chem.* **12,** 939–49 (2007).

18. Huber, M. M. *et al.* Fluorescently detectable magnetic resonance imaging agents. *Bioconjug. Chem.* **9,** 242–249 (1998).

19. Mulder, W. J. M. *et al.* Quantum dots with a paramagnetic coating as a bimodal molecular imaging probe. *Nano Lett.* **6,** 1–6 (2006).

20. Zhang, L. *et al.* Nanoparticles in Medicine : Therapeutic Applications and Developments. *Clinical pharmacology and therapeutics* **83,** 761–769 (2008).

21. Farokhzad, O. C. & Langer, R. Nanomedicine: Developing smarter therapeutic and diagnostic modalities. *Adv. Drug Deliv. Rev.* **58,** 1456–1459 (2006).

22. Na, H. Bin, Song, I. C. & Hyeon, T. Inorganic Nanoparticles for MRI Contrast Agents. *Adv. Mater.* **21,** 2133–2148 (2009).

23. Sharma, P., Brown, S., Walter, G., Santra, S. & Moudgil, B. Nanoparticles for bioimaging. *Adv. Colloid Interface Sci.* **123-126,** 471–85 (2006).

24. Bünzli, J.-C. G. Lanthanide luminescence for biomedical analyses and imaging. *Chem. Rev.* **110,** 2729–55 (2010).

25. Scaff, W., Dyer, D. & Mori, K. Fluorescent europium chelate stain. *J. Bacteriol.* **98,** 1–4 (1969).

26. Uh, H. & Petoud, S. Novel antennae for the sensitization of near infrared luminescent lanthanide cations. *Comptes Rendus Chim.* **13,** 668–680 (2010).

27. Fontes, A., Lira, R. & Seabra, M. in (2012). Quantum dots in biomedical research

28. Bruchez, M., Moronne, M., Gin, P., Weiss, S. & Alivisatos, a P. Semiconductor nanocrystals as fluorescent biological labels. *Science* **281,** 2013–6 (1998).

29. De, M., Ghosh, P. S. & Rotello, V. M. Applications of Nanoparticles in Biology. *Adv. Mater.* **20,** 4225–4241 (2008).

30. Ferreira, M. F. *et al.* Gd(DO3A-N-alpha-aminopropionate): a versatile and easily available synthon with optimized water exchange for the synthesis of high relaxivity, targeted MRI contrast agents. *Chem. Commun. (Camb).* 6475–7 (2009). doi:10.1039/b912201j

31. Ferreira, M. F. *et al.* Gold nanoparticles functionalised with stable, fast water exchanging Gd3+ chelates as high relaxivity contrast agents for MRI. *Dalton Trans.* **41,** 5472–5 (2012).

32. Bernstein, M. A., King, K. E., Zhou, X. J. & Fong, W. Handbook of MRI Pulse Sequences. *Med. Phys.* **32,** 1452 (2005).

33. Corsi, D. M., Platas-Iglesias, C., Bekkum, H. Van & Peters, J. a. Determination of paramagnetic lanthanide(III) concentrations from bulk magnetic susceptibility shifts in NMR spectra. *Magn. Reson. Chem.* **39,** 723–726 (2001).

34. Peters, J., Huskens, J. & Raber, D. Lanthanide induced shifts and relaxation rate enhancements. *Prog. Nucl. Magn. …* **28,** 283–350 (1996).

35. Barge, A. & Cravotto, G. How to determine free Gd and free ligand in solution of Gd chelates. A technical note. *Contrast media …* **188,** 184–188 (2006).

36. Aime, S., Botta, M., Ermondi, G., Fasano, M. & Terreno, E. Paramagnetic water proton relaxation enhancement: From contrast agents in MRI to reagents for quantitative "in vitro" assays. in *Magn. Reson. Imaging* **10,** 849–854 (1992).

37. Aime, S. *et al.* Conformational and Coordination Equilibria on DOTA Complexes of Lanthanide Metal Ions in Aqueous Solution Studied by (1)H-NMR Spectroscopy. *Inorg. Chem.* **36,** 2059–2068 (1997).

38. Hermann, P., Kotek, J., Kubícek, V. & Lukes, I. Gadolinium(III) complexes as MRI contrast agents: ligand design and properties of the complexes. *Dalton Trans.* 3027–3047 (2008). doi:10.1039/b719704g

39. Liu, S. The role of coordination chemistry in the development of target-specific radiopharmaceuticals. *Chem. Soc. Rev.* **33,** 445–461 (2004).

40. Kotek, J., Elst, L. Vander, Muller, R. N., Hermann, P. & Lukes, I. Pyridine- N -oxide Analogues of DOTA and Their Gadolinium (III). **48,** 455–465 (2009).

41. Polásek, M. *et al.* Lanthanide(III) complexes of pyridine-N-oxide analogues of DOTA in solution and in the solid state. A new kind of isomerism in complexes of DOTA-like ligands. *Inorg. Chem.* **48,** 466–75 (2009).

42. Polásek, M. *et al.* Lanthanide(III) complexes of a pyridine N-oxide analogue of DOTA: exclusive M isomer formation induced by a six-membered chelate ring. *Chem. Commun. (Camb).* **2,** 2602–3 (2004).

43. Keizers, P. H. J., Saragliadis, A., Hiruma, Y., Overhand, M. & Ubbink, M. Design, synthesis, and evaluation of a lanthanide chelating protein probe:

CLaNP-5 yields predictable paramagnetic effects independent of environment. *J. Am. Chem. Soc.* **130,** 14802–12 (2008).

44. Liu, W.-M. *et al.* A pH-sensitive, colorful, lanthanide-chelating paramagnetic NMR probe. *J. Am. Chem. Soc.* **134,** 17306–13 (2012).

45. Martins, A. F. *et al.* A Bis(pyridine N-oxide) Analogue of DOTA: Relaxometric Properties of the Gd(III) Complex and Efficient Sensitization of Visible and NIR-Emitting Lanthanide(III) Cations Including Pr(III) and Ho(III.). *Chemistry* (2014). doi:10.1002/chem.201403856

46. Schipper, M. L. *et al.* microPET-based biodistribution of quantum dots in living mice. *J. Nucl. Med.* **48,** 1511–1518 (2007).

47. Daneshvar, H. *et al.* Imaging characteristics of zinc sulfide shell, cadmium telluride core quantum dots. *Nanomedicine (Lond).* **3,** 21–29 (2008).

48. Koole, R. *et al.* Magnetic quantum dots for multimodal imaging. *Wiley Interdiscip. Rev. Nanomedicine Nanobiotechnology* **1,** 475–491 (2009).

49. Archer, P. I., Santangelo, S. a & Gamelin, D. R. Direct Observation of sp-d exchange interactions in colloidal Mn^{2+}- and Co^{2+}-doped CdSe quantum dots. *Nano Lett.* **7,** 1037–43 (2007).

50. Jin, T. *et al.* Gd^{3+}-functionalized near-infrared quantum dots for in vivo dual modal (fluorescence/magnetic resonance) imaging. *Chem. Commun. (Camb).* 5764–6 (2008). doi:10.1039/b812302k

51. Jokerst, J. V & Gambhir, S. S. Molecular imaging with theranostic nanoparticles. *Acc. Chem. Res.* **44,** 1050–60 (2011).

52. Reiss, P. ZnSe based colloidal nanocrystals: synthesis, shape control, core/shell, alloy and doped systems. *New J. Chem.* **31,** 1843 (2007).

53. Carvalho, K. H. G. *et al.* Fluorescence Plate Reader for Quantum Dot-Protein Bioconjugation Analysis. *J. Nanosci. Nanotechnol.* **14,** 3320–3327 (2014).